Modelling and evaluating different multi-carrier energy system configurations for a Dutch house

Alpízar-Castillo, Joel; Ramírez-Elizondo, Laura M.; Bauer, Pavol

Important note
To cite this publication, please use the final published version (if applicable).
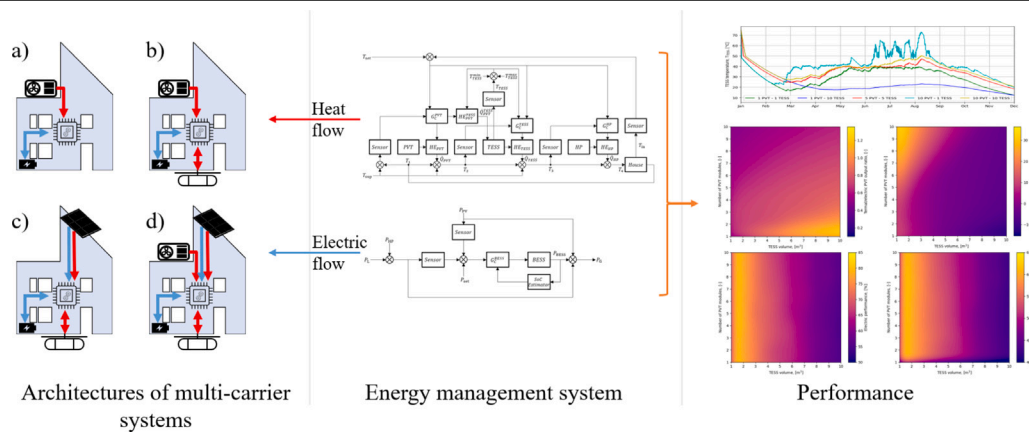Please check the document version above.

Modelling and evaluating different multi-carrier energy system configurations for a Dutch house

Joel Alpízar-Castillo *, Laura M. Ramírez-Elizondo, Pavol Bauer

Delft University of Technology, Mekelweg 6, Delft, 2628 CD, The Netherlands

GRAPHICAL ABSTRACT

Architectures of multi-carrier systems

Energy management system

Performance

ARTICLE INFO

ABSTRACT

The urge to reduce the dependence on natural gas for heating at the residential level has led to the deployment of different fossil fuel-free alternatives. In the Netherlands, two technologies are leading the transition: heat pumps, due to their high COP, and photovoltaic–thermal systems, due to their dual electric-thermal output. However, both represent a challenge for users and grid operators, aside from their stochastic behavior. Heat pumps alone can surpass a typical Dutch house's total energy and power consumption. Photovoltaic–thermal systems, as their only electric homologs, usually have a mismatch between generation and demand, causing energy injections to the grid. From the electric perspective, storage systems are a proven solution to reduce the energy exchange with the distribution network. This paper proposes four multi-carrier energy system configurations for a Dutch household, comprising different combinations of a photovoltaic–thermal system, a battery energy storage, a heat pump, and an underground water tank thermal energy system, providing analytical models for every component (including the thermal losses from the thermal storage to the ground), and the space heating and electrical demands. We determined the components' compatibility and evaluated the combinations considering their thermal performance, electrical performance, and equivalent CO_2 emissions. The results suggest that using a heat pump combined with a photovoltaic system and a battery provides the best trade-off. The photovoltaic–thermal system alone could not supply the thermal demand required for comfortable space heating nor reach temperatures high enough to charge the thermal storage. Combining the thermal storage with the heat pump allows a certain degree of flexibility for the heat pump activation

 * Corresponding author.
   E-mail address: j.j.alpizarcastillo@tudelft.nl (J. Alpízar-Castillo).

at the cost of COPs between 0.8 and 1.38 when used to charge the thermal storage, thus increasing energy consumption and equivalent emissions considerably.

Nomenclature

(k)	Current timestep
$(k + i)$	ith timestep in the future
$(k - i)$	ith timestep in the past

Abbreviations

BESS	Battery energy storage system
DRES	Distributed renewable energy sources
EMS	Energy management systems
ESS	Energy storage systems
HP	Heat pump
MCES	Multi-carrier energy system
PV	Photovoltaic
PVT	Photovoltaic thermal
RES	Renewable energy sources
TESS	Thermal energy storage System

Variables

$\dot{m}$	Mass flow
$\dot{Q}_D$	Thermal demand for space heating
$\dot{Q}_i^j$	Thermal power from the ith element to the jth element
$\dot{Q}_i$	Thermal power from the ith element to the thermal network
$\dot{Q}_L$	Thermal losses through walls, windows and roof
$\dot{Q}^{SD}$	TESS self-discharge
E^{SD}	BESS self-discharge
E_i	ith element electric energy stored
G	Solar irradiance
P	ith element electric power
Q_i	ith element thermal energy stored
t	Time
T_i	ith element temperature
v	Wind speed
y	Depth underground
COP	HP coefficient of performance
RH	Relative humidity
SoC_i	ith element state-of-charge

1. Introduction

Heat generation in residential buildings consumed 13% of the total energy consumption in the Netherlands in 2018 [1]. In response, the government has promoted the transition to fossil fuel-free alternatives, as 96% of Dutch households still use gas for heating [2]. Two main approaches are considered to diminish the usage of boilers: the deployment of fifth-generation district heating networks and directly replacing the gas boilers with other equipment that does not consume gas. The former was studied in [3], proposing an optimal sizing for the components in a case study in the north of the Netherlands. The latter approach includes multiple alternatives, such as heat pumps (HP), photovoltaic–thermal (PVT), infrared panels, and, more recently, thermal energy storage systems (TESS). This work focused on studying the second approach, considering only alternatives that use a hydraulic

network for space heating, specifically photovoltaic–thermal systems, heat pumps, and thermal energy storage systems.

Photovoltaic–thermal modules combine the advantages of solar collectors and photovoltaic systems; they can generate electric and thermal power simultaneously. Although the initial intention of coupling a heating exchange mechanism was to improve the PV cell efficiency, during the last decade, the frequency of studies related to PVT systems has grown considerably, given their opportunities to provide heat to other systems [4]. There are many classifications for PVT modules, but the working principle is essentially the same for them. A fluid (gas or liquid) circulates through a heat exchanger in the PVT module, extracting the heat from direct radiation, ambient temperature, or both [5]. Then, the fluid circulates through another heat exchanger to release the heat absorbed from the module. The review presented by [5] shows the evolution of electrical and thermal efficiencies from 2009 to 2019, showing ranges of electrical efficiencies from 6.4 to 28% and thermal efficiencies ranging from 27 to 79%, resulting in total efficiencies between 45 and 91%. Nevertheless, most of the literature uses simplified models to estimate the energy balance without considering the transport phenomena within the module in detail [6,7].

Thermal energy storage has been explored to increase the efficiency and reliability of thermal networks [8]. More specifically, [9] studied the actors related to deploying such systems in the Dutch context, including different configurations. Some authors like [10,11] have coupled thermal energy storage systems to heat pumps to minimize their electrical consumption. This kind of thermal energy storage application is called pumped thermal energy storage or Carnot batteries [12]. On the other hand, authors such as [13,14] studied how coupling a PVT system with a HP through a water tank can increase the system's overall performance. In their work, the water tank is referred to as thermal energy storage; however, due to its capacity, it mainly works as a buffer for short-term demand peaks, but it cannot sustain the supply for periods longer than a few hours. In our work, we consider this tank an intrinsic component of the PVT system, as detailed in Section 2.3. Phase-changing materials have also been used to improve the efficiency of PVT modules [15]. Units of such materials added to the PVT modules are also referred to as thermal energy storage [16] or thermal energy storage units [17]. When adding any type of thermal energy storage, most of the literature (excluding the phase-change materials attached directly to the PVT) locates the storage device indoors [18]. To avoid confusion with the terminology, this work considers *thermal energy storage* only the systems that can provide thermal power directly to the thermal network to supply the demand.

Heat pumps are the leading technology in residential heating electrification. They rely on a fluid with boiling points lower than typical outdoor temperatures. After boiling, the gas is compressed to increase its temperature. The hot gas then provides heat through a heat exchanger, to finally be depressurized, causing it to condense and restart the cycle. Thanks to this operation principle, they tend to be 3 to 4 times more efficient than fossil fuel boilers [19]. Still, there are many heat pump technologies reported in the literature. Some use ground heat exchangers, like coils, U pipes, and boreholes, which were compared in [20]. Air source technologies use evaporators in contact with the environment, which require less infrastructure costs than the ground heat exchangers but at the cost of more variable temperatures, reducing the COP of the device in cold climates [21]. For this reason, research is also required on working fluids [22] and alternatives to increase the temperature at the evaporator, for example, coupling a PVT system, as mentioned before.

However, literature [23] suggests that deploying heat pumps in low-voltage distribution networks can cause challenges in maintaining a stable and reliable network due to their high power consumption.

Simultaneously, it might worsen the instability conditions caused by distributed renewable energy sources (DRES), like photovoltaic (PV), as, on the one hand, high penetration of DRES in the low-voltage networks leads to overvoltages, as the surplus of power not consumed by the users is sent back to the grid. On the other hand, the power peaks of the HP alone are higher than the typical residential load, which might cause undervoltages. This combination, if not addressed promptly, can lead to severe congestion in the network.

One possible solution is to minimize the power exchange directly at the household level, including electrical or thermal energy storage systems. A combination of two or more different forms of energy is called a multi-carrier or multi-energy system. For instance, a PV and a battery energy storage system (BESS) would be a single carrier, whereas changing the PV to a PVT adds a thermal subsystem, resulting in a multi-carrier system. Recent works have demonstrated multi-carrier systems' opportunities to provide flexibility [24,25]. However, due to the novelty of these systems, there is no standard terminology. Some literature refers to multi-carrier systems as hybrid [7]. However, the word "hybrid" has been used for multiple connotations, even within the context of energy engineering. For example, [26] refers to one or more generators (*e.g.*, PV, hydro or diesel) coupled with a storage system as a hybrid system, [27] refers to a PVT system as a hybrid photovoltaic system combined with heat exchangers, and [28] calls hybrid energy storage to the couple of two different energy storage systems (in this case, BESS and hydrogen). In our work, we use the term multi-carrier energy systems (MCES) to avoid confusion with the terminology.

This paper determined the contributions of a heat pump, a PVT system and an underground thermal storage, as part of a multi-carrier energy system, to meet the space heating and electric demands for a household in the Netherlands. The thermal losses of the TESS to the ground were modeled, and four device combinations, comprised of devices with different sizes were compared in terms of energy consumption from the grid, thermal comfort and equivalent $CO_{2,eq}$ emissions. To elaborate on the current state-of-the-art of different asset configurations, we performed a comprehensive search using Scopus. We searched for previous work in multi-carrier energy systems using combinations of the terms: "photovoltaic thermal", "heat pump", "thermal energy storage", and "battery energy storage", as well as their respective acronyms, *i.e.*, PVT, HP, TES, and BESS. We included the different ways of writing the terms using wildcards and chose only results available in English. After the first search, it became apparent that numerous publications use PVT for desalination, phase change materials to enhance the output of PVT systems, and combined BESS with HP in electric vehicles (including buses and ships); thus, we excluded those terms in the second query. We also excluded works dedicated exclusively to sizing the components instead of analyzing their interactions. Then, we classified the results depending on the application and presented a summary in Table 1, including the number of publications found per combination and some examples.

1.1. Paper contributions

The literature review suggested that research has focused on residential applications. Of the 95 papers found, 64 correspond to residential, whereas for industrial and utility applications, we found 13 and 18, respectively. Most of the work regarding residential applications includes heat pumps as part of the overall system architecture, demonstrating their role in the energy transition and the challenges related to their limitations in conditions with lower temperatures. It was found that PVT systems and TESS are frequently used as support devices for the heat pump. In the case of TESS, they are usually water tanks with volumes below 1 m^3, thus can be located inside the house. However, TESS require higher volumes to provide sustained thermal power for space heating. To avoid occupying valuable space indoors, the TESS can be located underground outside the house, but this alternative still has to be studied in terms of thermal losses to the soil. In addition,

it is often assumed that the heat pumps would drastically reduce the equivalent emissions of the heating system compared to systems with gas boilers. However, emission contributions from increased use of the energy network still have to be investigated. This way, three main research gaps arise: the inclusion of PVT and TESS as part of the main thermal network and not as support devices, the effects of locating TESS underground outside the house, and the real equivalent emissions associated with heating electrification in residential buildings through heat pumps. In our work, we evaluated multiple multi-carrier energy system architectures comprising a PVT, a HP, a TESS, and a BESS for household applications (including different sizes of PVT and thermal energy storage systems). Based on the research gaps found, our contributions are:

1. determining the thermal contributions of including photovoltaic thermal and underground thermal energy storage systems into a residential space heating network,
2. proposing a mathematical model for an underground water tank thermal energy storage system considering the soil's temperature gradient,
3. evaluating the suitability of a MCES comprised of different combinations of a PVT, a HP, a TESS, and a BESS for household applications, based on electrical consumption from the grid, thermal power generation for space heating, and equivalent CO_2 emissions, and
4. making available a modular open-access model in Python to simulate a house, considering any combination of space heating and electric demands, a photovoltaic–thermal system, a heat pump, an underground thermal energy storage system, and a battery energy storage system, provided outdoor temperature, desired indoor temperature profile and electric load profile.

2. System description

The thermal network of the proposed multi-carrier energy system considers a water tank thermal energy storage system, a PVT, and a heat pump to meet the space heating thermal demand. Sections 2.1 to 2.5 present a discrete analytical model for each component, allowing us to couple them into a thermal network model. A similar approach is done for the electric carrier of the system. We considered a PVT and a battery energy storage system that, supported by the grid, can meet the base electric demand plus the heat pump consumption, which are described from Sections 2.6 to 2.9. Most of these models are validated in the literature; thus, we dedicated Section 3.1 to validate the thermal demand, the PVT and the underground TESS, using data available of measurements for those systems. Note that the models in this paper can be extrapolated to other case scenarios provided adequate constant values. Finally, we studied four different combinations of the components to determine their suitability for combined residential electric and thermal loads. We used the electric, thermal and equivalent emission performances to determine the best combination.

2.1. Thermal demand

For this work, we only considered space heating as thermal demand. Domestic hot water is another category of residential thermal loads. The work in [47] demonstrated that domestic hot water accounts for up to 2135 kWh/year in medium-sized European residences. However, the interaction with the overall system is different. Normally, domestic hot water requires high thermal power during short periods [18] and has a separate thermal network [48]. As this work focuses on the space heating thermal network, the thermal demand of domestic hot water will not be studied. We used an approach similar to [49] to model a house. The house comprises four rooms with specific thermal masses and losses to the environment through walls, double-glass windows and

Table 1

Previous research in residential multi-carrier energy systems containing PVT, HP, TESS, BESS, or their combination.

Combination	Publications	Examples	Year	Contribution
PVT, HP	17	Zhou et al. [29]	2020	Four PVT modules, a 150 L tank, and a HP were coupled, resulting in an average heating power of 4.7 kW and a COP of 6.16, under the environmental conditions of Northern China.
		Hengel et al. [30]	2020	A simulation of a PVT coupled to the regenerator of the HP with TRNSYS suggested higher performance than a HP alone and electric output 4.2% higher than a PV. However, the additional costs of the PVT do not compensate for the benefits.
PVT, TESS	1	Jiang et al. [31]	2022	Using a sorption TESS, it was possible to achieve energy efficiencies up to 38% in Hangzhou, China, 33% in Helsinki, Finland, and 35% in Copenhagen, Denmark.
HP, TESS	19	Renaldi et al. [32]	2017	A design and operational optimization for a HP paired with a TESS in the UK demonstrated that the equipment and operational costs of the HP system alone are higher than traditional heating systems, but integrating a TESS and using time-of-use tariffs reduce the operational costs to a competitive range.
		Aunedi and Strbac [33]	2022	Using the National Grid's Future Energy Scenarios of the United Kingdom, the benefit of installing TESS alongside HP at the residential level has system values between £1.1–2.3 bn/year in 2050, with annual long-term benefits per customer between £200–300. Also, TESS can considerably reduce the peak loading of heating electrification by as much as 2.3 GW at 50% TESS uptake.
PVT, HP, TESS	4	Vallati et al. [34]	2023	A residential building was modeled using Simulink demonstrated that reducing the temperature required at the could source of the HP increases the fraction of thermal energy produced by the PVT stored in the TESS 6%/°C, and increasing the capacity of the TESS increases the fraction of load covered by the PVT by up to 30%.
		ur Rehman et al. [35]	2022	Several technologies were simulated using TRNSYS to determine their integration with a building with seven floors and 51 apartments in Helsinki, Finland. The results suggest that the physical boundaries of the buildings might limit the amount of renewables needed to generate the power to supply the demand in Nordic countries, requiring the usage of extended or virtual boundaries of the building.
		Kim et al. [36]	2021	A TESS coupled with a HP was evaluated when combined either with PVT or solar collectors, simulating in TRNSYS a case study in Busan, Korea. The solar collectors were able to provide 27% of the annual cooling, heating, and domestic hot water demand, whereas the PVT covered 9%. The PVT produced 19.1% less electrical power than a PV due to continuous low temperatures.
PVT, BESS	11	Herrando et al. [37]	2018	A system was optimally sized and simulated for conditions in Athens, Greece, London, United Kingdom, and Zaragoza, Spain. The results covered up to 65% of the electric demand and 60, 30, and 45% of the thermal demand, respectively, displacing 3.87, 1.65, and 1.54 tons of $CO_{2,eq}$. The payback times were 15.6 years in Athens and 11.6 in Zaragoza.
		Abdul-Ganiyu et al. [38]	2021	PV and PVT systems were modeled and tested in Ghana. A techno-economic analysis over 25 systems suggests that the PVT performs better than the PV despite having higher initial costs, as the levelized cost of exergy is 0.33 US$/kWh for the PVT and 0.45 US$/kWh for the PV when installed with BESS.
		Gholami et al. [39]	2015	A system was simulated for Khuznin, Iran, suggesting that covering the thermal and electrical demands would require an over-dimensioned BESS.
HP, BESS	–	–	–	–
TESS, BESS	2	Rostmnezhad and Dessaint [40]	2023	A power management system with reinforcement learning, a BESS and TESS were controlled for peak shaving, achieving a 42.2% reduction in the BESS capacity.
		Brahman et al. [41]	2015	A demand response program was simulated for a residential energy hub, including load shifting and curtailing, and flexible storage usage, leading to cost savings of up to 40%.
PVT, HP, BESS	2	Koch and Dott [42]	2019	A residential building was simulated using Matlab/Simulink in Central Europe. HP performance increases when coupled with the PVT system.
		Izquierdo and de Agustín-Camacho [43]	2015	An experimental setup was deployed in Spain and tested from December 2012 to April 2013. The HP had a maximum COP of 6, with an average of 3.2. The overall system saved between 574 to 836 kg of $CO_{2,eq}$, depending on the type of boiler used as reference.
PVT, TESS, BESS	–	–	–	–
HP, TESS, BESS	8	Hyvönen et al. [44]	2022	Detached houses in southern Finland were simulated to evaluate the advantages of multi-carrier energy storage. The possibility of selling surplus energy stored in BESS improves the profitability to a renewable fraction of 20% for 2019 and 50% for 2021. However, hydrogen and TESS resulted in less profitable scenarios than using the grid unless sustained high market prices or subsidies are present.
		Efkarpidis et al. [45]	2022	Different control algorithms for multi-carrier systems were evaluated, highlighting the performance of the self-consumption maximization prioritizing the TESS over the BESS.
		Banaei et al. [46]	2021	A multi-objective approach for peak-shaving and flexibility capacity was proposed, minimizing user costs and equipment degradation, tested with 2000 cases of buildings, resulting in an energy bill increase of less than 0.5%, a peak demand reduction of 11%, and increased flexibility capacity of 16.5%.
PVT, HP, TESS, BESS	–	–	–	–

the roof, as shown in Fig. 1. Each room's internal energy change can be calculated with

$$\frac{dU}{dt} = \sum_{i=1}^{n} \dot{Q}_i = \sum_{i=1}^{n} \frac{d\,(m\,c\,T)_i}{dt}\,. \tag{1}$$

Since we do not consider any mass exchange between the exterior and interior of the house, one can rewrite (1) as

$$\frac{\Delta T}{\Delta t} \sum_{i=1}^{n} m_i\, c_i = \sum_{i=1}^{n} \dot{Q}_i\,; \tag{2}$$

thus,

$$\frac{\Delta T_{\text{in}}}{\Delta t} \sum_{i=1}^{n} m_i\, c_i = \dot{Q}_{\text{PVT}} + \dot{Q}_{\text{TESS}} + \dot{Q}_{\text{HP}} - \dot{Q}_{\text{D}}\,, \tag{3}$$

where $\dot{Q}_{\text{D}}$ includes the heat losses to the environment (thermal demand), $\dot{Q}_{\text{PVT}}$ the heat supplied by the PVT, $\dot{Q}_{\text{TESS}}$ the heat supplied by the thermal energy storage and $\dot{Q}_{\text{HP}}$ the heat supplied by the heat pump. m_i and c_i are the thermal mass of the air in the room, the walls, the roof and windows, and their specific heats, respectively. ΔT_{in} is the change in the room temperature during the timestep Δt. Thus, the temperature in the room can be approximated as:

$$T_{\text{in}}\,(k+1) = T_{\text{in}}\,(k) + \frac{\Delta t\left[\dot{Q}_{\text{PVT}}\,(k) + \dot{Q}_{\text{TESS}}\,(k) + \dot{Q}_{\text{HP}}\,(k) - \dot{Q}_{\text{D}}\,(k)\right]}{\sum_{i=1}^{n} m_i\, c_i}\,. \tag{4}$$

The heat transfer between rooms, to the ground, and radiative heat transfer are neglected. Although radiative heat through the windows can provide some heat to the inside of the house, this heat would be more significant during the Summer, when heating is less likely to be needed. In this work, we do not consider cooling mechanisms.

Each room's overall heat transfer coefficient depends on the conductive and convective losses, as shown in Fig. 1. Note that the conductive losses are divided into two identical sections with half of the distance, as we modeled the thermal mass in between. This coefficient can be calculated as

$$U = \left(\sum_{i=1}^{n} \frac{1}{h_i} + \sum_{i=1}^{m} \frac{L_i}{k_i}\right)^{-1}\,, \tag{5}$$

where h_i are the convection heat transfer coefficients, k_i the materials' conductivity and L_i the thickness of the convective materials. This way, the heat losses of the house to the environment through the walls, roof and windows can be calculated as:

$$\dot{Q}_L\,(k) = \sum_{i=1}^{n} U_i\, A_i\, \Delta T\,(k)\,, \tag{6}$$

where U_i and A_i are the total convection heat transfer coefficient and the surface area, respectively, and ΔT is the temperature difference between the outside and the inside of the house.

On the other hand, the losses through ventilation and infiltration can be calculated following the method presented in [50]. In both cases, the equation is governed by the air mass exchange inside and outside the house. The ventilation losses $\dot{Q}_v$ can be calculated as:

$$\dot{Q}_v\,(k) = c_a \rho_a q_v \Delta T\,(k)\,, \tag{7}$$

where c_a and ρ_a are the specific heat capacity and density of the air, $\Delta T\,(k)$ the temperature difference between the outside and inside of the house (in degree Fahrenheit). To estimate the required ventilation airflow q_v (in cubic feet per minute), [50] suggest using

$$q_v = 0.03 A_{\text{cf}} + 7.5\left(N_{\text{br}} + 1\right)\,, \tag{8}$$

where A_{cf} is the building conditioned area (in feet squared) and N_{br} is the number of bedrooms in the house. Similarly, the infiltration losses can be estimated with

$$\dot{Q}_i\,(k) = c_a \rho_a q_i \Delta T\,(k)\,. \tag{9}$$
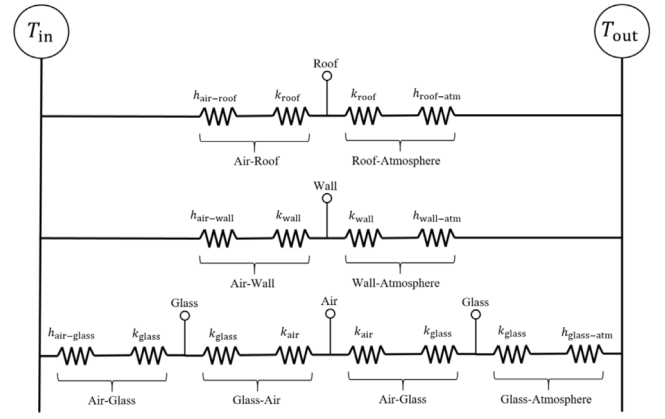
Fig. 1. Convective and conductive thermal losses through the roof, walls, and windows considered per house room.

The infiltration airflow q_i can be estimated using

$$q_i\,(k) = A_{\text{es}} A_u \sqrt{C_s |\Delta T\,(k)| + C_w u^2\,(k)}\,, \tag{10}$$

where A_{es} is the building's exposed area (in feet squared), A_u is the unit leakage area (in inches squared per feet squared), C_s is the stacking coefficient, C_w is the wind coefficient and u is the wind speed (in miles per hour).

In addition, buildings can have internal sources of heat. In residential buildings, the occupants of the building and appliances like stoves, ovens and incandescent lighting could contribute to increasing the temperature. We considered a two-person house with highly efficient appliances, induction cooking and LED lighting; thus, internal heat gains can be neglected in this case [50]. This way, the total thermal demand of the house is

$$\dot{Q}_D = \dot{Q}_L + \dot{Q}_v + \dot{Q}_i \tag{11}$$

2.2. Thermal energy storage system

We considered an underground, perfectly mixed water tank as the thermal energy storage system. To model the tank, we performed a similar analysis as in Section 2.1, i.e., we did not consider any mass exchange between the TESS and the heating system of the house or with the ground; thus, (1) can be rewritten as:

$$\dot{Q}_{\text{PVT}}^{\text{TESS}}\,(k) - \dot{Q}_{\text{TESS}}\,(k) - \dot{Q}^{\text{SD}}\,(k) = \sum_{i=1}^{n} m_i c_i \frac{\Delta T_{\text{TESS}}}{\Delta t}\,, \tag{12}$$

where $\dot{Q}_{\text{PVT}}^{\text{TESS}}$ is the heat supplied by the solar collectors to charge the TESS, $\dot{Q}_{\text{TESS}}$ the heat supplied by the thermal energy storage to the thermal demand, m_i and c_i are the thermal mass fluid in the TESS and the walls and their specific heats, respectively, and ΔT_{TESS} is the change in the TESS temperature during the timestep Δt. Thus, one can use

$$T_{\text{TESS}}\,(k+1) = T_{\text{TESS}}\,(k) + \frac{\Delta t\left[\dot{Q}_{\text{PVT}}^{\text{TESS}}\,(k) + \dot{Q}_{\text{TESS}}^{\text{TESS}}\,(k) - \dot{Q}_{\text{TESS}}\,(k) - \dot{Q}^{\text{SD}}\,(k)\right]}{\sum_{i=1}^{n} m_i c_i}\,, \tag{13}$$

to approximate the temperature of the TESS.

The charge $\dot{Q}_{\text{TESS}}^{\text{c}}$ or discharge power $\dot{Q}_{\text{TESS}}$ are

$$\dot{Q}_{\text{TESS}}^{\text{c}}\,(k) = \eta_{\text{TESS}}^{c}\,(k)\, \dot{m} c_{\text{f}} \Delta T\,, \tag{14}$$

and

$$\dot{Q}_{\text{TESS}}\,(k) = \eta_{\text{TESS}}^{d}\,(k)\, \dot{m} c_{\text{f}} \Delta T\,, \tag{15}$$

where η_{TESS} is the charge or discharge efficiency as corresponds, $\dot{m}$ is the mass flow through the heat exchangers of the TESS, c_{f} is the fluid

specific heat capacity, and ΔT is the temperature difference between the inlet and outlet of the heat exchanger. In our case, we considered a TESS with separated charge and discharge coils; therefore, the TESS can be charged and discharged simultaneously. During the charge, we considered the outlet temperature to be the same as the fluid in the tank. During the discharge, we considered an output temperature equal to the supply temperature of the thermal network.

The thermal energy stored in the tank can be expressed as

$$Q_{\text{TESS}}(k) = C_{\text{TESS}} SoC_{\text{TESS}}(k) , \tag{16}$$

and its capacity C_{TESS} as

$$C_{\text{TESS}} = \rho_f V c_f \left(T^{\max} - T^{\min} \right) , \tag{17}$$

where ρ_f is the fluid density, V is the tank volume, and $T^{\max}$ and $T^{\min}$ are the maximum and minimum temperatures allowed in the tank. As there are no changes in the fluid's mass or composition, the state-of-charge of the TESS depends only on its temperature, *i.e.*,

$$SoC_{\text{TESS}} = \frac{C_{\text{TESS}}(k)}{C_{\text{TESS}}} = \frac{\Delta T(k)}{\Delta T^{\max}} = \frac{T(k) - T^{\min}}{T^{\max} - T^{\min}} . \tag{18}$$

where $T(k)$ is the current temperature of the fluid.

The self-discharge of the tank, $\dot{Q}^{\text{SD}}$, is produced by the heat transferred to the soil around the tank. Fig. 2(a) shows a diagram of the losses considered for the tank. We considered the soil's temperature constant at any specific depth y. This way, convective heat transfers from the water to the tank's walls and conductive heat from the walls to the soil. To determine the soil's temperature, we modeled it as a semi-infinite solid with one-dimensional coordinates, as proposed by [51,52]. The heat diffusion in the soil follows the equation

$$\frac{\partial^2 T_s(y,t)}{\partial y^2} = \frac{1}{\alpha} \frac{\partial T_s(y,t)}{\partial t} . \tag{19}$$

Using the finite difference method to discretize the equation, the space-dependent side of (19) can be rewritten using central differencing as

$$\frac{\partial^2 T_s(y,t)}{\partial y^2} = \frac{T_s(y - \Delta y, k) - 2T_s(y,k) + T_s(y + \Delta y, k)}{\Delta y^2} . \tag{20}$$

Similarly, using forward differencing, the time-dependent side of (19) can be rewritten as

$$\frac{\partial T_s(y,t)}{\partial t} = \frac{T_s(y, k+1) - T_s(y,k)}{\Delta t} . \tag{21}$$

This way, and gathering the time Δt between timesteps, the grid size squared Δy^2, and the thermal diffusivity of the soil α as

$$r = \frac{\alpha \Delta t}{\Delta y^2} , \tag{22}$$

(19) can be reorganized as

$$T_s(y, k+1) = r \left[T_s(y - \Delta y, k) - 2T_s(y,k) + T_s(y + \Delta y, k) \right] + T_s(y,k) \tag{23}$$

The boundary conditions for (23) are the temperatures at the surface and at a point underground, at a depth d, with a known and constant temperature. The first boundary condition can be obtained by considering Fourier's Conductivity Law, Newton's Law of Cooling, and Stefan–Boltzmann's Law of Radiation, resulting in

$$-k_{\text{soil}} \frac{\partial T_s(y,t)}{\partial y} = h \left[T_{\text{amb}}(t) - T_s(y=0,t) \right] - \varepsilon \Delta R(t) + \alpha_0 G(t) , \tag{24}$$

where T_{amb} is the ambient temperature, $T(y=0,t)$ is the temperature at the surface, ε is the soil's thermal emissivity, α_0 is the soil's diffusivity, G is the solar radiation and

$$\Delta R(t) = \sigma \left[T_s^4(t - \Delta t) - T_{\text{sky}}^4(t) \right] \tag{25}$$

is the thermal radiation. There are many empirical expressions to estimate the sky temperature. For this paper, we considered the recalibrated Brunt model

$$T_{\text{sky}}(t) = 0.62 + 0.056 \left[6.11 \left(\frac{RH}{100} \right) e^{\left(\frac{17.63 T_{\text{amb}}(t)}{243.04 + T_{\text{amb}}(t)} \right)} \right]^{0.5} \tag{26}$$

as a widely used expression to estimate the sky temperature [53], where RH is the relative humidity.

The total heat transfer coefficient h can be written as

$$h(t) = h^{\text{conv}}(t) + h^r(t) , \tag{27}$$

where

$$h^{\text{conv}}(t) = \begin{cases} 5.7 + 3.8\, v_w(t) & \forall\, v_w \in [0, 5[\ \text{m/s} \\ 6.47 + v_w^{0.78}(t) & \forall\, v_w \in [5, 10[\ \text{m/s} \end{cases} \tag{28}$$

corresponds to the coefficient of convective heat transfer, depending on the wind speed v_w, and

$$h^r(t) = \varepsilon \sigma \left[T_s^2(t - \Delta t) + T_{sky}^2(t) \right] \left[T_s(t - \Delta t) + T_{sky}(t) \right] \tag{29}$$

corresponds to the coefficient of radiant heat transfer [54].

Discretizing the Fourier term in (24) as

$$-k_{\text{soil}} \frac{\partial T_s(y,t)}{\partial y} = -k_{\text{soil}} \frac{T_s(y=d,t) - T_s(y=0,t)}{d} , \tag{30}$$

allows to obtain the discrete expression for the temperature at the surface at any timestep

$$T_s(y=0,k) = \frac{k_{\text{soil}} T_s(y=d,k) + dh T_{\text{amb}}(k) - d\varepsilon \Delta R(k) + d\alpha_o G(k)}{dh + k_{\text{soil}}} , \tag{31}$$

or in terms of the effective temperature T_e

$$T_s(y=0,k) = \frac{k_{\text{soil}} T_s(y=d,k) + dh T_e(k)}{dh + k_{\text{soil}}} , \tag{32}$$

where

$$T_e(k) = T_{\text{amb}}(k) - \frac{\varepsilon \Delta R(k)}{h} + \frac{\alpha_o G(k)}{h} \tag{33}$$

The second boundary condition for (23) is the annual mean effective temperature, $\bar{T}_e$. This temperature is found at a point underground, where the effects at the surface and the geothermal heating are neglectable. We considered this point at a depth of 6 m [51].

Given the above, we can use (6) to estimate the heat lost by the TESS to the ground as

$$\dot{Q}^{\text{SD}} = \dot{Q}^{\text{SD}}_{\text{top}} + \dot{Q}^{\text{SD}}_{\text{sides}} + \dot{Q}^{\text{SD}}_{\text{bottom}} . \tag{34}$$

Considering a constant temperature for the top and bottom walls of the tank, $T_s(y=y_0,k)$ and $T_s(y=y_f,k)$, respectively, and a discrete gradient of temperature in the soil, $T_s(y_i,k)$ where $y_i \in \{y_0 + L_{\text{TESS}}, y_0 + L_{\text{TESS}} + \Delta y, \ldots, y_f - L_{\text{TESS}}\}$, as shown in Fig. 2(b), the components of (34) are

$$\dot{Q}^{\text{SD}}_{\text{top}} = U_{\text{TESS}} A_{\text{top}} \left[T_{\text{TESS}}(k) - T_s(y=y_0,k) \right] , \tag{35}$$

$$\dot{Q}^{\text{SD}}_{\text{sides}} = \sum_{i=1}^{n} U_{\text{TESS}} A_{\Delta y} \left[T_{\text{TESS}}(k) - T_s(y_i,k) \right] , \tag{36}$$

and

$$\dot{Q}^{\text{SD}}_{\text{bottom}} = U_{\text{TESS}} A_{\text{bottom}} \left[T_{\text{TESS}}(k) - T_s(y=y_f,k) \right] . \tag{37}$$

2.3. Photovoltaic–thermal system

We used a similar approach to model the PVT module as [54]. However, we defined a different grouping strategy for the constants in the equations and considered the tank and the modules connected in series as part of a hydraulic system. The model considers a layered PVT module, as shown in Fig. 3(a), and includes reflective, radiative,
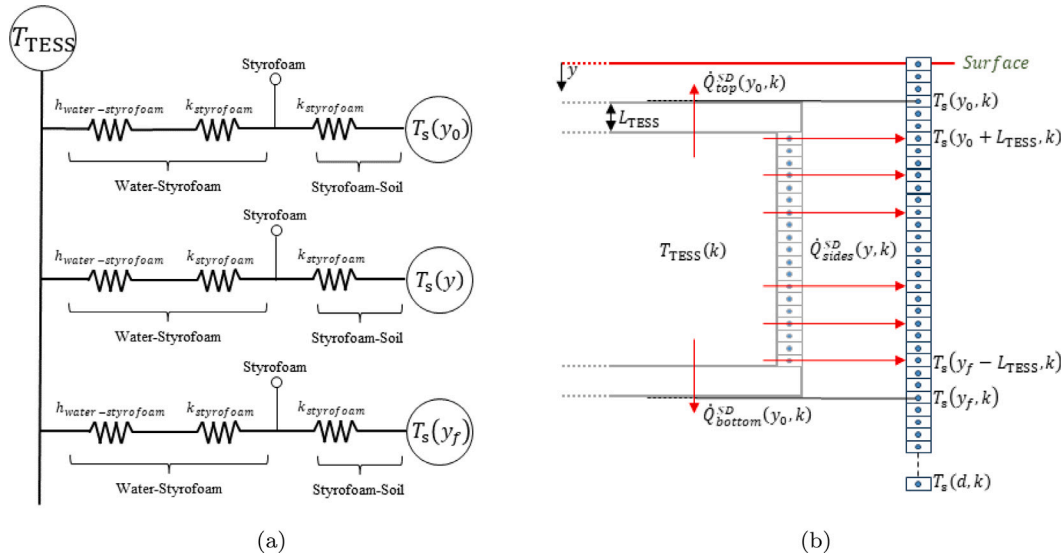
Fig. 2. Thermal model used for the TESS. (a) Conductive thermal losses through the walls. (b) Discrete representation.

convective, and conductive losses, as shown in Fig. 3(b). Note that the PV layer comprises glass, two layers of EVA, the Si cell, and a Tedlar layer. The governing equations of the model, as a function of the surface temperatures of the glass cover, the Si cell, the thermal absorber, and the fluid, T_{glass}, T_{PV}, T_a and T_f, respectively, are

$$\begin{cases} T_{\text{glass}}(k+1) = C_1(k)T_{\text{glass}}(k) + C_2(k)T_{\text{PV}}(k) - D_1(k) \\ T_{\text{PV}}(k+1) = C_3(k)T_{\text{glass}}(k) + C_4(k)T_{\text{PV}}(k) + C_5(k)T_a(k) - D_2(k) \\ T_a(k+1) = C_6(k)T_{\text{PV}}(k) + C_7(k)T_a(k) + C_8(k)T_f(k) - D_3(k) \\ T_f(k+1) = C_9(k)T_a(k) + C_{10}(k)T_f(k) - D_4(k) \end{cases},$$

(38)

where

$$C_1(k) = \frac{A_{\text{glass}}\Delta t}{m_{\text{glass}}c_{\text{glass}}}\left[\frac{m_{\text{glass}}c_{\text{glass}}}{A_{\text{glass}}\Delta t} - h_{\text{glass}}^{\text{conv}}(k) - h_{\text{glass}}^r(k) - h_{\text{gap}}(k) - h_{\text{glass-PV}}^r(k)\right],$$

(39)

$$C_2(k) = \frac{A_{\text{glass}}\Delta t}{m_{\text{glass}}c_{\text{glass}}}\left[h_{\text{gap}}(k) + h_{\text{glass-PV}}^r(k)\right],$$

(40)

$$C_3(k) = \frac{A_{\text{PV}}\Delta t}{m_{\text{PV}}c_{\text{PV}}}\left[h_{\text{gap}}(k) + h_{\text{glass-PV}}^r(k)\right],$$

(41)

$$C_4(k) = \frac{A_{\text{PV}}\Delta t}{m_{\text{PV}}c_{\text{PV}}}\left[\frac{m_{\text{PV}}c_{\text{PV}}}{A_{\text{PV}}\Delta t} - h_{\text{gap}}(k) - h_{\text{glass-PV}}^r(k) - h_{\text{PV-a}}^{\text{cond}}(k)\right],$$

(42)

$$C_5(k) = \frac{A_{\text{PV}}\Delta t}{m_{\text{PV}}c_{\text{PV}}}h_{\text{PV-a}}^{\text{cond}}(k),$$

(43)

$$C_6(k) = \frac{A_a\Delta t}{m_a c_a}h_{\text{PV-a}}^{\text{cond}}(k),$$

(44)

$$C_7(k) = \frac{\Delta t}{m_a c_a}\left[\frac{m_a c_a}{\Delta t} - h_{\text{PV-a}}^{\text{cond}}(k)A_a - h_{\text{a-f}}(k)A_t^{\text{cross}} - h_a^{\text{cond}}(k)A_a\right],$$

(45)

$$C_8(k) = \frac{\Delta t}{m_a c_a}h_{\text{a-f}}(k)A_t^{\text{cross}},$$

(46)

$$C_9(k) = \frac{A_t^{\text{cross}}\Delta t}{m_f c_f}h_{\text{a-f}}(k),$$

(47)

$$C_{10}(k) = \frac{\Delta t}{m_f c_f}\left[\frac{m_f c_f}{\Delta t} - h_{\text{a-f}}(k)A_t^{\text{surf}} - 2\dot{m}_f c_f\right],$$

(48)

$$D_1(k) = \frac{A_{\text{glass}}\Delta t}{m_{\text{glass}}c_{\text{glass}}}\left[h_{\text{glass}}^{\text{conv}}T_{\text{amb}}(k) + h_{\text{glass}}^r(k)T_{\text{sky}}(k) + \alpha_{\text{glass}}G(k)\right],$$

(49)

$$D_2(k) = \frac{A_{\text{PV}}\Delta t}{m_{\text{PV}}c_{\text{PV}}}\alpha_{\text{PV}}\tau_{\text{glass}}G(k)\left[1 - \eta_{\text{PV}}(k)\right],$$

(50)

$$D_3(k) = \frac{A_a\Delta t}{m_a c_a}h_a^{\text{cond}}(k)T_{\text{amb}}(k),$$

(51)

and

$$D_4(k) = 2\frac{\Delta t}{m_f}\dot{m}_f T_f^{\text{in}}(k).$$

(52)

The nomenclature for parameters of the Eqs. (39)–(52) is as follows: h_{i-j}^{cond} and h_{i-j}^r represent the conductive and radiative thermal coefficients from the ith to the jth layer, respectively, h_i and h_i^{conv} represent the total thermal coefficient and the convective thermal coefficient (released to the environment) for the ith layer. A_i, m_i, c_i, L_i, α_i and τ_i are the area, mass, specific heat, thickness, absorbance and transmittance of the ith layer. A_t^{cross} is the tube's cross area (in contact with the thermal absorber), and A_t^{surf} is the tube's lower surface area (in contact with the isolation layer). G is the solar radiation and η_{PV} is the PV cell efficiency.

In this case $h_{\text{glass}}^{\text{conv}}$ can be calculated using (28), h_{glass}^r using (29), and h_{gap} using (5) for the convective heat transfer through the glass and the first layer of EVA, and

$$h_{\text{glass-PV}}^{\text{conv}}(k) = \frac{\text{Nu}_{\text{gap}}k_{\text{gap}}}{L_{\text{gap}}},$$

(53)

for the convective term, where Nu_{gap} and k_{gap} are the Nusselt number and thermal conductivity of the air. The radiative heat transfer coefficient between the glass and the PV layer can be calculated with

$$h_{\text{glass-PV}}^r(k) = \frac{1}{\frac{1}{\varepsilon_{\text{glass}}} + \frac{1}{\varepsilon_{\text{PV}}} - 1}\sigma\left[T_{\text{glass}}^2(k-1) + T_{PV}^2(k-1)\right]$$

$$\times\left[T_{\text{glass}}(k-1) + T_{PV}(t-\Delta)\right].$$

(54)

The conductive heat transfer coefficient through the layers of the PV (glass, EVA, Si cell and tedlar) to the thermal absorber, $h_{\text{PV-a}}^{\text{con}}$, can be calculated using the conductive component of (5) [55]. The heat transfer coefficient between the fluid and the thermal absorber depends
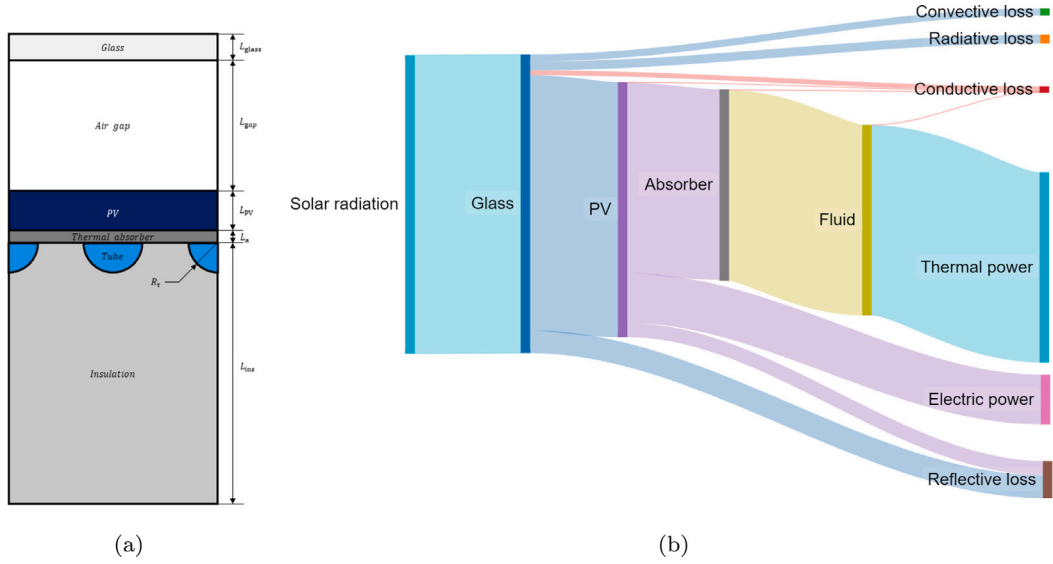
Fig. 3. Representation of the thermal model for the PVT. (a) Schematic of the PVT layers. (b) Heat transfer and loss distribution.

on the flow and can be calculated as

$$h_{\text{a-f}}(k) = \begin{cases} 2\dfrac{k_{\text{f}}}{D_{\text{H}}} & \forall \, \text{Re} = 0 \\ 4.36\dfrac{k_{\text{f}}}{D_{\text{H}}} & \forall \, 0 < \text{Re} < 2300 \\ 0.023\dfrac{k_{\text{f}}}{D_{\text{H}}}\text{Re}^{0.8}\text{Pr}^{0.4} & \forall \, \text{Re} \geq 2300 \end{cases} \quad , \quad (55)$$

where D_{H} is the hydraulic diameter of the tube, and Re and Pr are the Reynolds and Prandtl numbers, respectively. For the fluid temperature in the tubes, we considered

$$T_{\text{f}}(k) = \frac{T_{\text{f}}^{\text{in}}(k) + T_{\text{f}}^{\text{out}}(k)}{2} \quad (56)$$

as the relation between the inlet and outlet temperatures, T_{f}^{in} and $T_{\text{f}}^{\text{out}}$. Last, as the PV efficiency depends on the PV temperature, it can be calculated using

$$\eta_{\text{PV}}(k) = \eta_{\text{PV}}^{\text{STC}}\left[1 - \beta_{\text{PV}}\left(T_{\text{PV}}(k) - T_{\text{ref}}\right)\right], \quad (57)$$

where $\eta_{\text{PV}}^{\text{STC}}$ is the PV efficiency under standard test conditions, and T_{ref} is the reference temperature for the standard test conditions.

Finally, the thermal power generated by the module can be expressed as

$$\dot{Q}_{\text{PVT, mod}}(k) = \eta_{\text{T}}N\dot{m}_{\text{f}}c_{\text{f}}\left[T_{\text{f}}^{\text{out}}(k) - T_{\text{f}}^{\text{in}}(k)\right] = 2\eta_{\text{T}}N\dot{m}_{\text{f}}c_{\text{f}}\left[T_{\text{f}}(k) - T_{\text{f}}^{\text{in}}(k)\right], \quad (58)$$

where η_{T} is the efficiency of the heat exchanger and N is the number of tubes in the PVT.

The PVT module generally uses fluids and mass flows different than the tank and the thermal network; thus, the heat transferred from the PVT system to the thermal network uses a water tank as the coupling device. In this case, the inlet temperature of the PVT module is the tank temperature. To estimate the temperature in the tank T_{PVT}, one can adapt (13) for the PVT system, resulting in

$$T_{\text{PVT}}(k+1) = T_{\text{PVT}}(k) + \frac{\Delta t\left[\dot{Q}_{\text{PVT, mod}}(k) - \dot{Q}_{\text{PVT}}(k) - \dot{Q}_{\text{PVT}}^{\text{TESS}}(k)\right]}{m_{\text{tank}}c_{\text{tank}}}, \quad (59)$$

where $\dot{Q}_{\text{PVT}}$ is the thermal power from the PVT system to the thermal network, and $\dot{Q}_{\text{PVT}}^{\text{TESS}}$ is the thermal power from the PVT system to the TESS.

2.4. Heat pump

As the PVT depends on the weather conditions, we included a heat pump to ensure at least one heat source when weather conditions are unfavorable and the TESS is unavailable. To model the behavior of the heat pump, we used

$$\text{COP}(k) = 7.90471e^{-0.024\left[T_{\text{ret}}(k) - T_{\text{amb}}(k)\right]} \quad (60)$$

as proposed by [56], where T_{ret} is the temperature of the working fluid at the inlet of the heat pump, and the constants were obtained after a lineal regression from 10 different models of residential heat pumps. Note that

The relation between the electric power consumption and the thermal power delivered by the HP is

$$P_{\text{HP}}(k) = \frac{\dot{Q}_{\text{HP}}(k)}{\text{COP}(k)}, \quad (61)$$

where the thermal power delivered by the HP is a function of the mass flow rate $\dot{m}_f$, the fluid specific heat c_f, the required supply temperature T_{sup} the return temperature T_{ret}, and the heat exchanger efficiency η_{HP} given by

$$\dot{Q}_{\text{HP}}(k) = \eta_{\text{HP}}\dot{m}_f c_f\left[T_{\text{sup}} - T_{\text{ret}}(k)\right]. \quad (62)$$

2.5. Thermal network

We coupled the thermal demand with the PVT, the TESS, and the HP using the thermal network shown in Fig. 4. From the thermal balance for the coupled system given in (3), one can approximate the return temperature at the different points of the network as

$$T_1(k) = T_4(k-1) - \frac{\dot{Q}_{\text{D}}(k-1)}{\dot{m}_f c_f}, \quad (63)$$

$$T_2(k) = T_4(k-1) + \frac{\dot{Q}_{\text{PVT}}(k) - \dot{Q}_{\text{D}}(k-1)}{\dot{m}_f c_f}, \quad (64)$$

$$T_3(k) = T_4(k-1) + \frac{\dot{Q}_{\text{PVT}}(k) + \dot{Q}_{\text{TESS}}(k) - \dot{Q}_{\text{D}}(k-1)}{\dot{m}_f c_f}, \quad (65)$$

$$T_4(k) = T_4(k-1) + \frac{\dot{Q}_{\text{PVT}}(k) + \dot{Q}_{\text{TESS}}(k) + \dot{Q}_{\text{HP}}(k) - \dot{Q}_{\text{D}}(k-1)}{\dot{m}_f c_f}. \quad (66)$$

Given that (15), (58) and (62) depend on the inlet and outlet temperatures of the heat exchangers of the TESS and the HP, respectively,
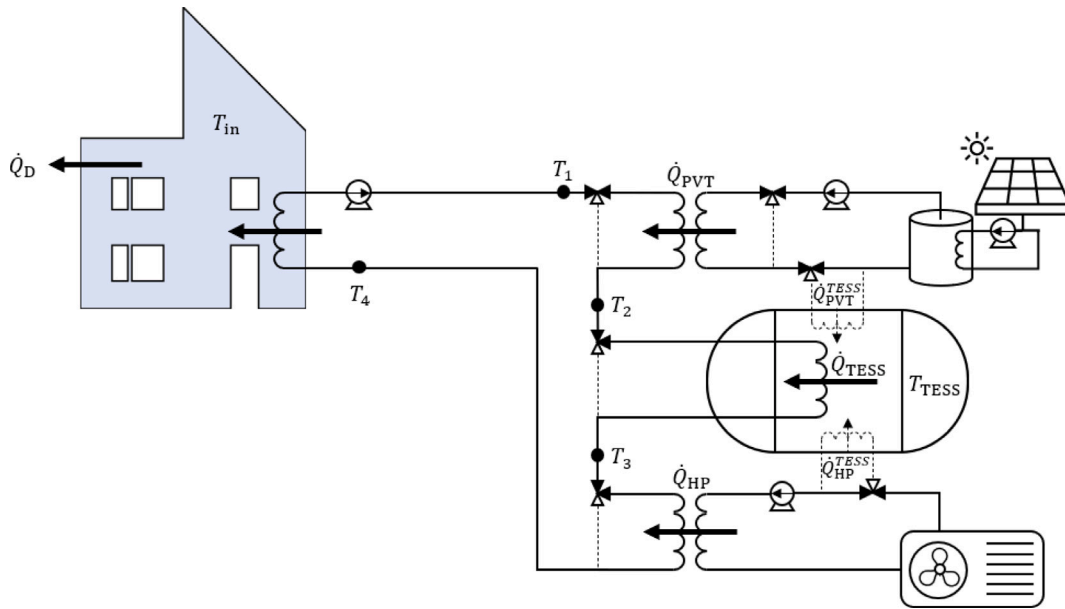
Fig. 4. Thermal network diagram.
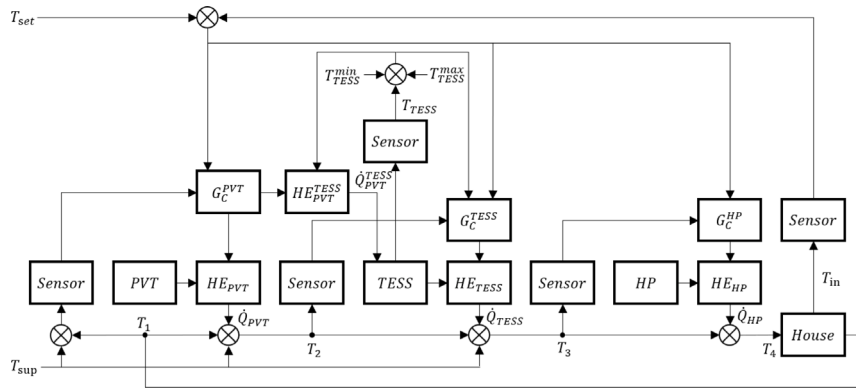
Fig. 5. Control strategy used by the EMS in the thermal carrier.
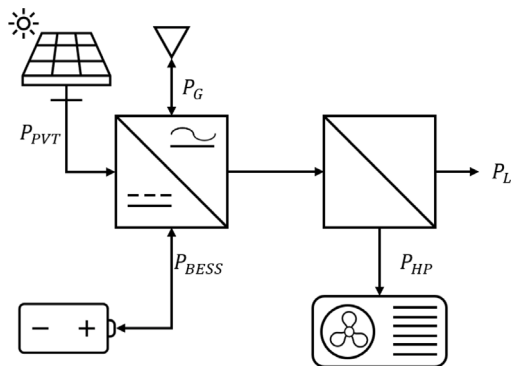
Fig. 6. Electric network diagram.

using (63)–(65), they can be rewritten as

$$\dot{Q}_{\text{TESS}}(k) = \eta^d_{\text{TESS}} \dot{m} c_f \left[T_{\text{sup}} - T_2(k) \right] , \qquad (67)$$

$$\dot{Q}_{\text{HP}}(k) = \eta_{\text{HP}} \dot{m}_f c_f \left[T_{\text{sup}} - T_3(k) \right] . \qquad (68)$$

$$\dot{Q}_{\text{PVT}} = 2\eta_{\text{PVT}} N \dot{m}_f c_f \left[T_f(k) - T_1(k) \right] , \qquad (69)$$

The energy management system uses the cascade control shown in Fig. 5. First, it evaluates the indoor temperature; if it is above the setpoint, no heating is needed. Suppose the indoor temperature is below the setpoint. In that case, the control evaluates the temperatures T_1, T_2 and T_3, as the supply temperature to the domestic heating system, T_4, should be at least 50 °C. This way, the PVT, TESS, or HP would add heat to the working fluid as needed.

2.6. Electric demand

We created a synthetic load profile based on the power of different appliances and their probabilities of being used at the current timestep. Thus, the total electrical power demanded was calculated as

$$P_L(k) = \sum_{i=1}^{n} P_i(k) \, \mathbb{P}_i \left(\{ \omega_i(k) \in \Omega_i(k) \} \right) \qquad (70)$$

where P_i is the power for each appliance considered, and $\mathbb{P}_i$ and $\Omega_i(t)$ are the probability of that appliance to be used and the event space at the instant k, respectively, based on typical power consumptions [57].
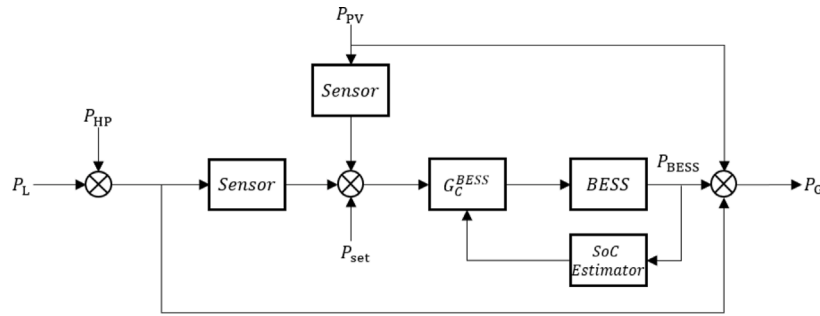
Fig. 7. Control strategy used by the EMS in the electric carrier.

Note that we do not consider the heat pump's power as part of the electrical demand of the house in (70), as it does not have a probabilistic behavior. Instead, it reacts to the thermal demand, following the EMS instructions.

2.7. Photovoltaic thermal system

In Section 2.3, we detailed the thermal model for the PVT modules used in this work. This model provides the temperature of the PV cell as a function of the ambient temperature, wind speed, and irradiance at any particular moment. Given the cell temperature, one can use

$$\eta_{\text{PV}}(k) = \eta_{\text{STC}} \left(1 - \beta \left[T_{\text{PV}}(k) - T_{\text{ref}} \right] \right) \tag{71}$$

to estimate the PV efficiency of the PVT, based on the environmental conditions, where η_{STC} and T_{ref} are the reference efficiency and temperature at standard test conditions. Therefore, the electrical power produced by a PVT module, with a total cell area A_{PV}, is

$$P_{\text{PV}}(k) = \eta_{\text{PV}}(k) A_{\text{PV}} G(k) . \tag{72}$$

2.8. Battery energy storage system

For the BESS, we considered Li-ion batteries. Consistently with most of the literature, we modeled them using an energy-balance approach. This way, the energy stored in the BESS at a particular moment depends on its previous state and the amount of power extracted or provided between sampling times [58], *i.e.*,

$$E_{\text{BESS}}(k) = C_{\text{BESS}}(k-1) SoC(k-1) + \frac{P_{\text{BESS}}(k)}{\eta^{\text{c,d}}(k)} \Delta t - E_{\text{BESS}}^{\text{SD}}(k) , \tag{73}$$

where E_{BESS} is the future amount of energy stored in the battery, C_{BESS} is the capacity of the battery, SoC is the state-of-charge of the battery, $\eta^{\text{c,d}}$ is the charge or discharge efficiency as correspond, P_{BESS} is the charge or discharge power as corresponds, Δt is the sampling time and $E_{\text{BESS}}^{\text{SD}}$ is the self-discharge of the battery between time samples.

2.9. Electric network

We considered a power electronics converter as the coupling point for the electric components, as shown in Fig. 6. For the EMS, we used the hierarchical self-consumption strategy proposed in [58], governed by the power balance equation

$$P_{\text{G}} - P_{\text{L}} - P_{\text{HP}} + P_{\text{PVT}} + P_{\text{BESS}} = 0 , \tag{74}$$

where P_{G} and P_{L} are the power purchased from the grid and the power consumed by the loads in the house. The control diagram is shown in Fig. 7. As can be seen, the algorithm will prioritize the PV generation, then the BESS, and, at last, the purchase from the grid. The charging and discharging powers of the BESS are constrained to the battery's inverter capacity

Table 2
Parameters used to simulate the BESS.

Parameter	Symbol	Value	Units
Capacity	E_{BESS}	3.36	kWh
Power	P_{BESS}	1.28	kW
Charge/Discharge efficiency	$\eta_{\text{c, d}}$	0.943	–
Minimum SoC	SoC_{min}	0.2	–
Maximum SoC	SoC_{max}	0.9	–

3. Results and discussion

This section presents the results of four different system architectures. First, we demonstrate the individual behavior of the thermal components and compare the results with reference values for systems with similar characteristics. Then, we classified the thermal components as controllable and non-controllable to create the different case scenarios. This way, the heat pump, and the thermal energy storage system are controllable, and the PVT is non-controllable, as it depends on the instantaneous meteorological conditions. However, it should be noted that the TESS cannot meet the thermal energy demand as a whole and should be coupled with an external energy source. This is because we considered water as its working fluid, which can store around 50 kWh/m^3 for the given temperature range, and the yearly space heating thermal demand is approximately 8207 kWh. For this reason, the only component robust enough to meet the thermal demand independently is the heat pump. Given the above, we will evaluate the following four scenarios:

- *Scenario I:* only heat pump.
- *Scenario II:* heat pump coupled with a thermal energy storage system (with two different charging protocols).
- *Scenario III:* a PVT system coupled with a thermal energy storage system (with two different charging protocols).
- *Scenario IV:* a PVT system coupled with a thermal energy storage system (with two different charging protocols) and a heat pump.

We evaluated all the cases using up to 10 PVT modules, TESS volumes up to 10 m^3 and a BESS. Tables 2, 3, 5 and 6, show the parameters used to model the system.

3.1. Individual behavior of the thermal components

In this work, we proposed analytical models for every component of the multi-carrier energy system. We used previously validated models for the heat pump, the battery storage system, and the electric demand. We modified models from previous research for the soil thermodynamics and the PVT. Finally, we proposed the models for the space heating thermal demand and the underground thermal energy storage system. This section is dedicated to validating the simulation results with data available on similar systems installed in the Netherlands.

Table 3

Parameters used to simulate the house [61].

Parameter	Symbol	Value				Units
		Roof (glass fiber)	Walls (concrete)	Windows (glass)	Windows (cavity)	
Density	ρ	2440	2400	2500	1.025	kg/m^3
Area	A	120.3	111.6	8	8	m^2
Thickness	L	0.2	0.25	0.004	0.014	m
Specific heat	c	835	750	840	1005.4	J/(kg-K)
Conductivity	k	0.04	0.14	0.8	0.0257	W/(kg-K)
Air specific heat	c_a	1012				J/(kg-K)
Air density	ρ_a	1.293				kg/m^3
No. of bedrooms	N_{br}	1				–
Exposed area	A_{es}	119.6				m^2
Unit leak area	A_u	0.01				in^2/ft^4
Stack coefficient	C_s	0.015				cfm^2/(in$^{4\circ}$ F)
Wind coefficient	C_w	0.0012				cfm^2/(in^{4}mph^2)
Time step	Δt	900				s

Table 4

Convective heat transfer coefficients used to simulate the house [61].

Interface	Value [W/(m^2-K)]
Indoor air - wall	0.9
Wall - atmosphere	0.9
Indoor air - window (glass)	25
Window (glass) atmosphere	32
Indoor air - roof	12
Roof - atmosphere	38

Table 5

Parameters used to simulate the TESS and its losses to the soil.

Parameter	Symbol	Value	Units
TESS			
Density (water)	ρ_f	1000	kg/m^3
Volume (water)	V_f	4	m^3
Specific heat (water)	c_f	4200	J/(kg-K)
Maximum temperature	T^{max}	95	°C
Minimum temperature	T^{min}	50	°C
Charge/Discharge efficiency	$\eta_{c,d}^{TESS}$	0.8	–
Area (top, bottom)	$A_{top, bottom}$	11.02	m^2
Discrete differential side area	$A_{\Delta y}$	0.134	m^2
Area (sides)	A_{sides}	21.44	m^2
Thickness (styrofoam)	L_{TESS}	0.314	m
Specific heat (styrofoam)	c_{styro}	1.34	J/(kg-K)
Conductivity (styrofoam)	k_{styro}	0.033	W/(kg-K)
Depth of the TESS top wall	y_0	0.2	m
Depth of the TESS bottom wall	y_f	1.8	m
Soil			
Thermal diffusivity	α_s	3.877×10^{-7}	–
Absorptivity	α_0	0.25	–
Emissivity	ϵ_s	0.25	–
Conductivity	k_s	1.19	W/(kg-K)
Density	ρ_s	2029.80	kg/m^3
Specific heat	c_s	1512.22	J/(kg-K)
Depth of the reference temperature	d	6	m
Grid size	Δy	0.01	m
Time step	Δt	60	s

3.1.1. Thermal demand

For this case, we simulated a 120 m^2 house built between 1990 and 2000, with an energy label C (using the Dutch energy efficiency standard) during 2021. The house is occupied by two adults and has highly efficient appliances and LED lighting. The parameters used are shown in Tables 3 and 4, and the weather data was retrieved from the Royal Netherlands Meteorological Institute database [59]. The free response of the indoor temperature (without any heating) is shown in Fig. 8(a). Then, we defined a setpoint for the comfortable temperature inside the house. The heat balance in the system should ensure the indoor temperature is at equal or higher than the temperature profile throughout the year. This temperature ranges from 20 °C between 6:00 and 22:00, and 17 °C for the remaining time. The thermal losses to the environment are shown in Fig. 8(b) when the indoor temperature matches the setpoint temperature, which adds 8207 kWh per year. We used the values of energy consumption reported by [49,60] as a reference, as they provide data for different types of houses in the Netherlands (including age and area). Our results suggest an average specific heat demand of 68.4 kWh/(m^2-year), which is between the reported range of 45 to 86 kWh/(m^2-year).

3.1.2. Thermal energy storage system

We modeled a 4 m^3 underground water tank TESS, located 0.2 m below the surface, using the parameters shown in Table 5, and the weather data from the Royal Netherlands Meteorological Institute database [59]. The thermal behavior of the soil is presented in Fig. 9, showing a more variable behavior in shallow depths, which is consistent with [62], [63] and [52]. For the TESS, we used a three-step test cycle. The TESS starts charged at 90 °C (SoC of 100%) and is left to discharge to 50 °C (SoC of 0%) due to self-discharge. Then, it is charged back to 90 °C using a constant charging temperature of 95 °C. Finally, it is discharged to 50 °C using a network temperature of 40 °C. The behavior of the temperature is shown in Fig. 10(a). As

expected, the isolation of the TESS walls kept the thermal power loss between 250 W and 140 W, proportional to the TESS temperature, causing a slow self-discharge during the first step of the test cycle (see Fig. 10(b)). During the second step, 250 kWh are used to charge the TESS, whereas 150 kWh can be retrieved from the TESS in the third due to the roundtrip efficiency of the heat exchanger (see Fig. 10(c)). Simultaneously, the charging and discharging steps had thermal losses of 13.14 and 6.72 kWh, respectively.

3.1.3. Photovoltaic–thermal system

To evaluate the PVT model, we simulated a system comprised of 10 modules in series during 2022; the parameters used are shown in Table 6. The HP is activated when the PVT cannot provide heat to meet the thermal demand. From the year, we selected a representative period
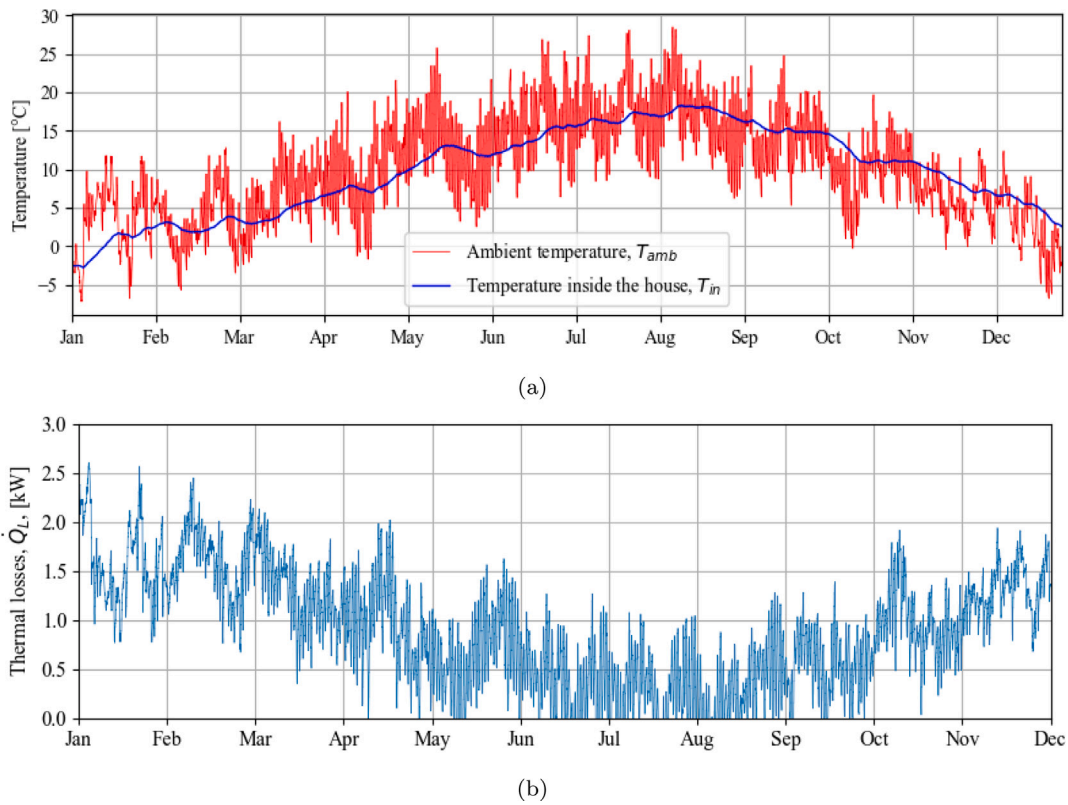
Fig. 8. Results of the thermal model of the house. (a) Indoor temperature behavior without thermal sources (b) Thermal losses when the indoor temperature follows the setpoint temperature.
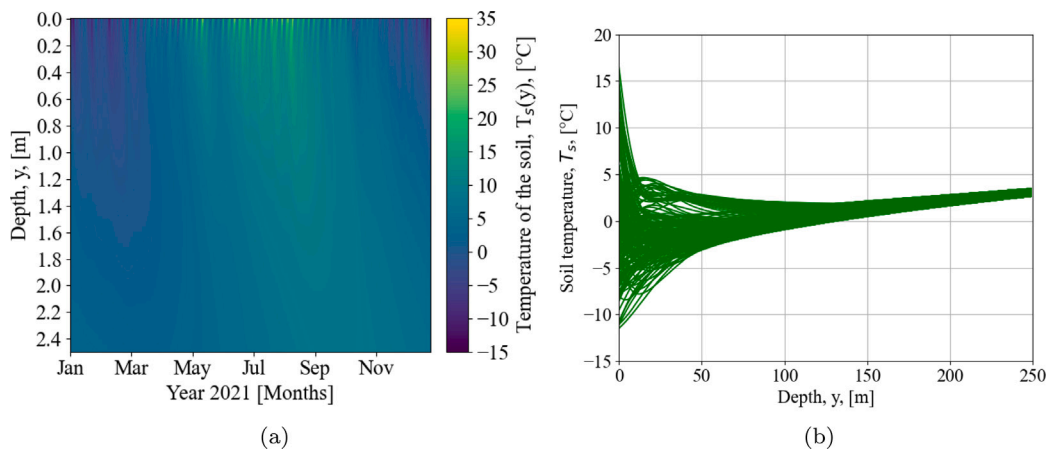
Fig. 9. Results of the thermal model of the soil for 2022. (a) Soil temperature throughout the year. (b) Soil temperature, measured every two days.
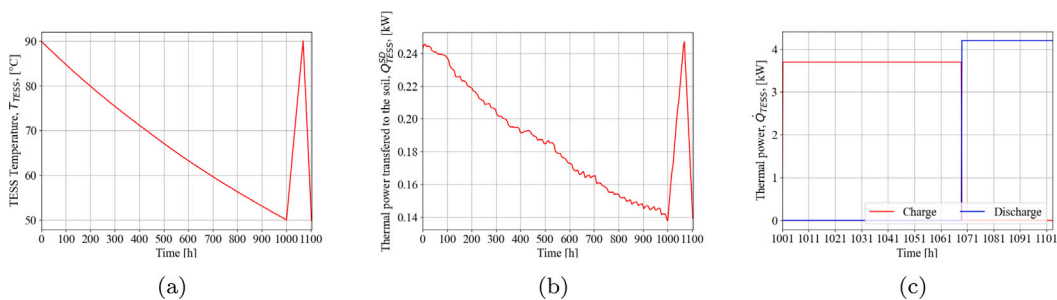
Fig. 10. Results of the test cycle for the TESS: (a) temperature, (b) Self-discharge, and (c) Charge and discharge powers during steps 2 and 3 of the test.

Table 6
Parameters used to simulate the PVT module.

Parameter	Symbol	Value	Units	Parameter	Symbol	Value	Units
Glass area	A_{glass}	1.48	m^2	Glass thermal conductivity	k_{glass}	1.8	W/(m-K)
PV area	A_{PV}	1.46	m^2	Air thermal conductivity	k_{glass}	0.024	W/(m-K)
Absorber area	A_a	1.48	m^2	PV glass thermal conductivity	k_{PV}	1.8	W/(m-K)
Tube area	A_t	1.48	m^2	PV EVA thermal conductivity	k_{PV}	0.35	W/(m-K)
Glass density	ρ_{glass}	2200	kg/m^3	PV tedlar thermal conductivity	k_{PV}	0.2	W/(m-K)
PV density	ρ_{PV}	2330	kg/m^3	Fluid thermal conductivity	k_f	0.6071	W/(m-K)
Absorber density	ρ_a	2699	kg/m^3	Insulation thermal conductivity	k_{ins}	0.035	W/(m-K)
Tube density	ρ_f	1050	kg/m^3	Glass specific heat	c_{glass}	670	J/(kg-K)
Glass thickness	L_{glass}	0.004	m	PV specific heat	c_{PV}	900	J/(kg-K)
Air gap thickness	L_{air}	0.02	m	Absorber specific heat	c_a	800	J/(kg-K)
PV glass thickness	L_{PV}	0.003	m	Fluid specific heat	c_f	3800	J/(kg-K)
PV EVA thickness	L_{PV}	0.0005	m	Glass diffusivity	α_{glass}	0.1	–
PV tedlar thickness	L_{PV}	0.0001	m	PV diffusivity	α_{PV}	0.9	–
Absorber thickness	L_a	0.001	m	Glass emissivity	$\varepsilon glass$	0.9	–
Insulation thickness	L_{ins}	0.04	m	PV emissivity	εPV	0.96	–
Mass flow	$\dot{m}_f$	0.029	kg/s	Glass transmittance	$\tau glass$	0.1	–
Tank mass	m_{tank}	200	kg	Heat exchanger efficiency	η_T	0.8	–
Time step	Δt	1	s	PV cell reference efficiency	η_{PV}	0.184	–
				PV temperature coefficient	β_{PV}	0.3	%/°C

from summer and winter to demonstrate the system's behavior under different weather conditions. In Fig. 11 we presented the temperature in the different layers of the PVT (glass, T_{glass}, PV cell, T_{PV}, absorber, T_a), of the fluid in the return of thermal network, T_{net}, of the fluid in the PVT tubes T_f and in the PVT tank, T_{PVT}, as a function of the global irradiance, G, and the ambient temperature, T_{amb}.

During summer, less thermal power is demanded due to higher temperatures. This is reflected in Fig. 11(a), as the PVT is not used during June 30 and July 1, despite the tank temperature being above the supply temperature, whereas from June 27 to 29 there are moments where thermal power is demanded, increasing the temperature in the network and reducing the temperature in the tank. In contrast, winter weather conditions do not allow the PVT to warm the tank above the supply temperature (see Fig. 11(b)); thus, the PVT cannot provide thermal power to the network, and the HP is activated. Still, both cases have similar temperature behaviors, increasing sharply when irradiance is available and decreasing slowly in its absence. Likewise, the temperature in the glass remains the coldest among the PVT layers, as it is exposed to the ambient, and the temperature in the PV cell and the absorber is near the same as they are in direct contact. Such results are consistent with [54].

3.2. Scenario I: Boiler vs. HP

We used a traditional natural gas boiler as a reference to evaluate the behavior of the traditional, gas-based heating system. The power required to keep the house above the setpoint temperature is depicted in Fig. 8(b), and consists of 8207 kWh per year. To estimate the amount of $CO_{2,eq}$ the boiler produces to supply the space heating thermal demand, we considered a 20 kW gas boiler with an efficiency of 92%, resulting in a total consumption of 601 kg (718 m^3) of natural gas, corresponding to 1497 kg of $CO_{2,eq}$, given the Dutch emission factor of 2.085 kg $CO_{2,eq}/m^3$. On the other hand, we evaluated using a fully electric heat pump as the thermal energy source. Using the model described in Section 2.4, the results showed a total electrical consumption of 5255 kWh, of which the heat pump consumed 2886 kWh. The COP of the heat pump ranged from 2.18 in colder days to 3.92 in warmer days throughout the

year. Considering the Dutch emission factor of 0.523 kg $CO_{2,eq}$ per kWh of energy, the heat pump operation produces 1509 kg of $CO_{2,eq}$.

3.3. Scenario II: HP and TESS

We considered two charging protocols for coupling the heat pump with a thermal energy storage system. The first protocol, called from now on *fully-charged*, keeps the SoC of the TESS as close to 100% as possible (90 °C), as shown in Fig. 12(a). This protocol minimizes the heat required from the heat pump, given that it depends on the difference between the temperature in the TESS and its maximum temperature (set as the charging temperature), as shown in (62). The second protocol, called *cycling*, leaves the TESS to discharge to 50 °C, then charges to the maximum SoC, as shown in Fig. 12(b), improving the COP since it depends on the difference between the TESS and ambient temperatures, as shown in (60).

To evaluate the performance of each charging protocol, we considered TESS sizes from 0 to 10 m^3 and proposed three indicators: the amount of energy lost to the soil due to self-discharge of the TESS, the ratio of thermal energy extracted from the TESS to the thermal energy stored, and the ratio of thermal energy extracted from the TESS to the required electrical energy used to generate the thermal energy stored in the TESS. We defined the first ratio as thermal performance and the second as electric performance; for both cases, the energy associated with the initial state of charge is excluded. The self-discharge results presented in Fig. 13(a) show an increasing trend in the accumulated energy lost to the soil with the volume of the TESS. This is related to the contact area of the tank with the soil since (35)–(37) establish a direct relationship between the thermal losses and the area of the TESS. Moreover, the fully-charged protocol keeps the TESS at a higher temperature, increasing the heat flux to the surrounding soil.

The thermal and electric performances for all considered TESS volumes are shown in Fig. 13(b). The results suggest a higher thermal performance for the fully-charged TESS protocol. The thermodynamics of the heat transfer can explain this, as the higher the temperature in the TESS, the easier the energy flows towards the thermal network. Nevertheless, keeping the TESS in a higher SoC requires a more frequent use of the HP, summed to a lower COP due to the higher
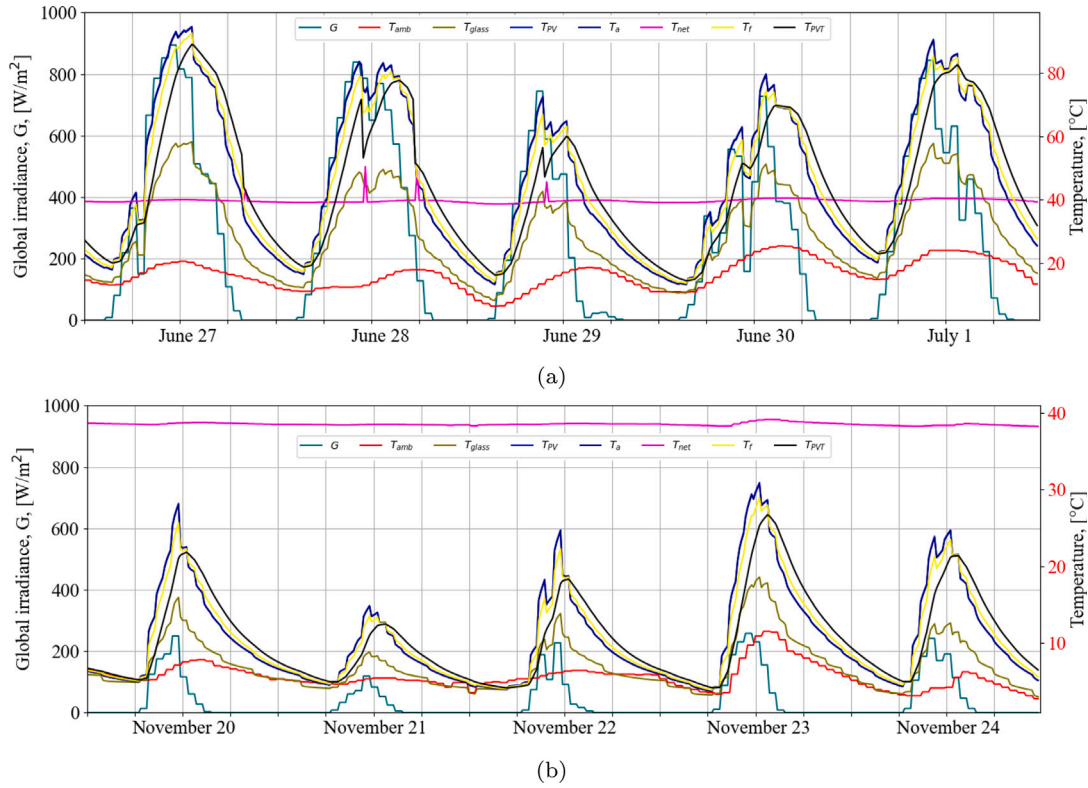
Fig. 11. Results of the thermal model of the PVT during (a) summer and (b) winter.
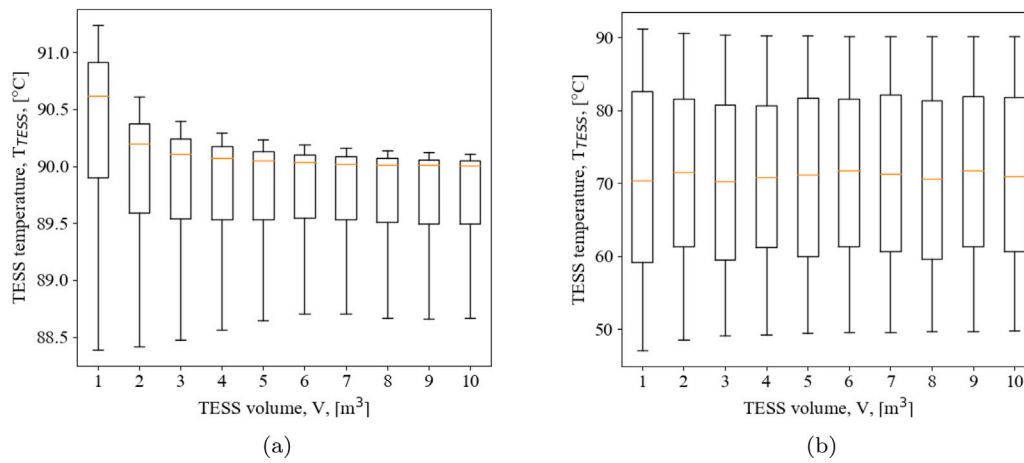
Fig. 12. Distribution of the temperature in the TESS when using the (a) fully-charged and (b) cycling protocols.

difference between the temperature required to heat the TESS and the ambient temperature. On the other hand, the cycling protocol leaves the TESS temperature to reach temperatures closer to the supply temperature required by the thermal network, leading to a slower response. However, the reduced frequency at which the HP is used and better COPs for most of the charging time result in better electric performance. Still, the COP for both protocols was very low, averaging 0.88 to 0.95 in the fully-charged protocol and 1.29 to 1.38 for the cycling protocol. In both cases, the smaller the capacity of the TESS, the higher the COP. Such low COPs lead to energy consumption several times the consumption of the HP in Section 3.2, as shown in Fig. 13(c). Similarly, the overall equivalent emissions also increase considerably, as shown in Fig. 13(d).

3.4. Scenario III: PVT and TESS

Solar-dependent technologies, such as PV or PVT, are usually unsuitable as stand-alone energy sources. Adding BESS or TESS, respectively, would allow the energy to be stored when there is no demand for the supply. Therefore, we evaluated the suitability of a PVT system combined with a TESS as an alternative to gas boilers. We considered TESS sizes from 0 to 10 m³, combined with PVT systems varying from 0 to 10 modules. The indicators we used for this scenario are: the number of days when the indoor temperature was below 16 °C at any moment, called "cold days", the energy lost to the soil due to self-discharge of the TESS, the thermal performance, and the ratio of thermal energy used from the PVT to the electrical energy produced.
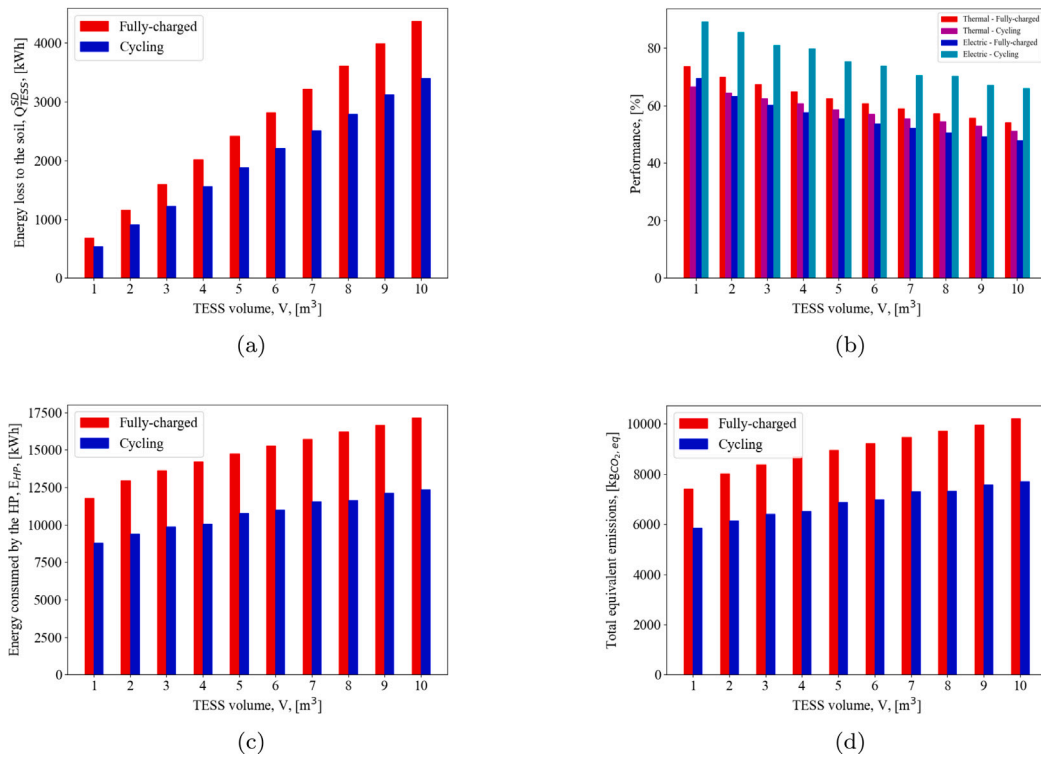
Fig. 13. Assessment of the energy performance of Scenario 2 for each charging protocol. (a) Energy loss to the soil due to self-discharge of the TESS. (b) Thermal and electric performance of the coupled system. (c) Electrical energy consumption of the HP. (d) Equivalent CO_2 emissions.

In this case, the results suggest that the combination is unsuitable due to the number of cold days shown in Fig. 14(a). One can notice that the number of cold days increases with the size of the TESS. This is because the thermal power from the PVT system used to charge the TESS reduces the temperature in the PVT tank. Therefore, when thermal power is required to heat the house, the temperature the PVT system can provide is lower than in the case without TESS. Likewise, the bigger the capacity of the TESS, the higher the heat absorption rate from the PVT, as it requires more thermal energy to increase the temperature. Additionally, as shown in Section 3.3, increasing the volume of the TESS increases the self-discharge rate. Thus, the overall system becomes less efficient.

The phenomenon is demonstrated by correlating the results in Figs. 14(b) and 14(c), where it is shown that the thermal energy sent from the PVT to the thermal network decreases. In contrast, the energy sent to the TESS increases when increasing the capacity of the TESS. Simultaneously, increasing the SoC of the TESS increases the energy lost due to self-discharge, as shown in Fig. 14(d). Fig. 14(e) shows the thermal energy supplied by the TESS, which is consistently lower than the thermal energy it received from the PVT. Note that increasing the temperature of the TESS sometimes requires less temperature than heating the house. As shown in Fig. 15, the temperature in the TESS reaches values below the supply temperature required to heat the house, allowing it to charge with lower temperatures from the PVT, increasing the amount of usable thermal energy from the PVT. Nonetheless, the performance of the system is poor.

As shown in Fig. 16(a), the TESS can only provide energy to the thermal network with small capacities and many PVT modules. The negative results account for the energy delivered from the initial state-of-charge (55%). Also, PVT's thermal production is consistently below its electrical production. As shown in Fig. 16(b), although it is generally mentioned that the thermal output of the PVT outperforms the electric counterpart, it depends on the required output temperature. The high temperatures demanded by the TESS diminish the thermal output of the PVT. The PVT can deliver thermal energy to the TESS only when it

reaches very low temperatures, which happens with higher capacities and few PVT modules and with small capacities and many PVT modules as shown in Fig. 15. However, the electrical output grows linearly with the number of modules, but this relationship is not valid for the thermal output. For this reason, the thermal performance is better with small capacities and many modules, and the thermal-to-electric output ratio is not optimal in that region.

From the electrical perspective, it is possible to achieve net-zero building when increasing the number of PVT modules. For this case, the base energy consumption is 2375 kWh/year, which can be achieved with 7 PVT modules, as shown in Figs. 17(a) and Fig. 17(b). However, the mismatch between instant production and consumption prevents the energy from being consumed immediately, urging energy storage to avoid sending energy back to the grid. In contrast with the previous scenarios, this one can benefit from a battery energy storage system. As shown in Fig. 17(c), the BESS can store up to one-third of the yearly energy consumption but saturates after the seventh PVT module. This is because, at that point, the energy generation is greater than the consumption, and the energy sent back to the grid increases proportionally to the generation, as shown in Fig. 17(d). At this point, congestion issues might emerge.

3.5. Scenario IV: PVT, TESS, and HP

This section evaluates the combination of all the components; however, only two of the five possible modes of operation are considered: the two charging protocols with the heat pump alone, without considering the PVT to charge the TESS. We based this decision on the results of the previous sections. In Section 3.3, we demonstrated that charging the TESS only with the HP has a trade-off between thermal and electrical performance, based on the charging protocol. However, it was possible to meet the thermal demand. Section 3.4, on the other hand, demonstrated that using the PVT to charge the TESS is not possible due to the low temperatures the PVT can achieve. For this reason, we exclude the three combinations that would use the PVT to
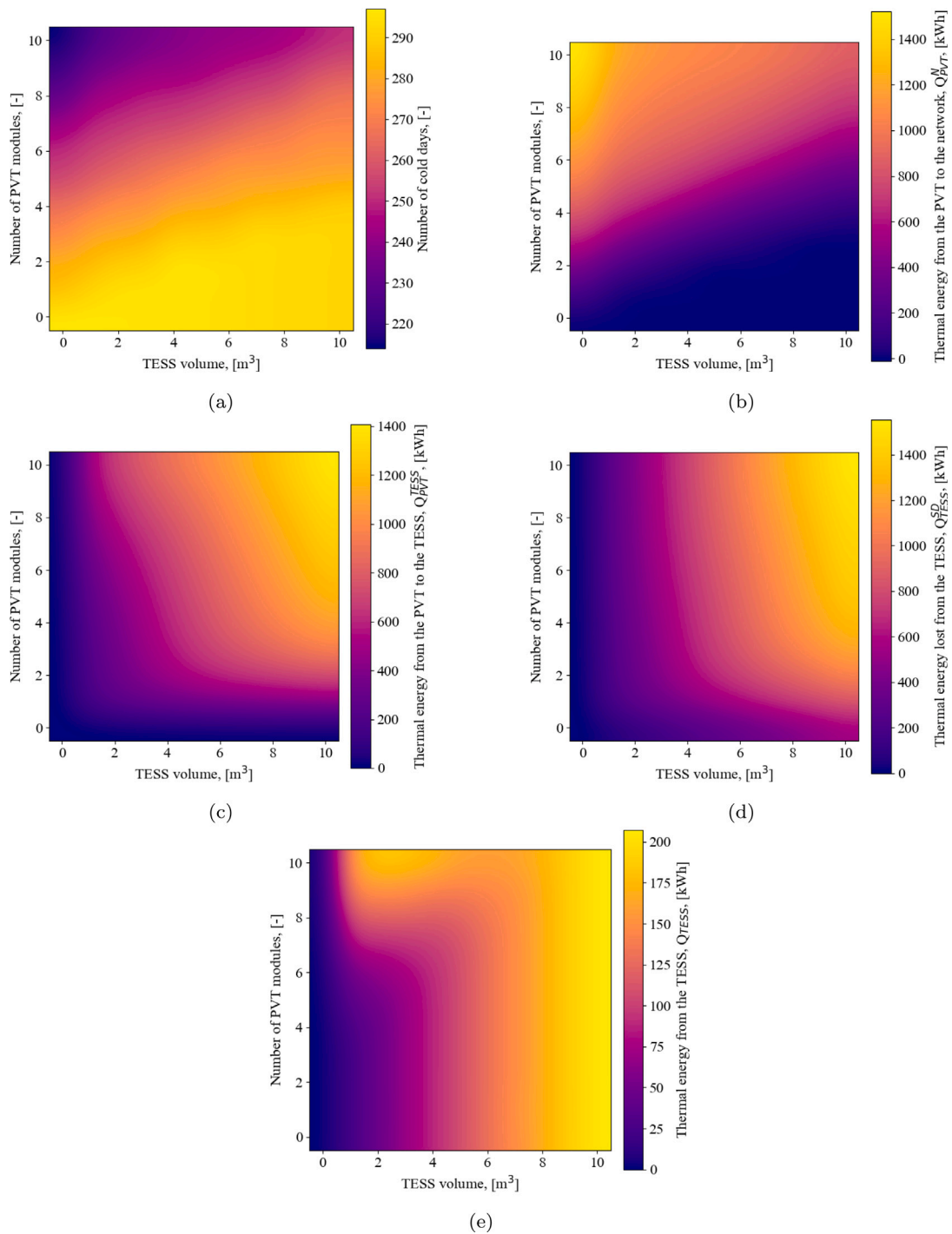
Fig. 14. Thermal power flow in Scenario 3. (a) Cold days. (b) Thermal energy from the PVT to the thermal network. (c) Thermal energy from the PVT is used to charge the TESS. (d) Energy loss to the soil due to self-discharge. (e) Thermal energy from the TESS to the thermal network.

charge the TESS, *i.e.*, using only the PVT, and using both the PVT and the HP with its two charging protocols. Thus, the indicators are the same as Section 3.4.

We first evaluated the role of the PVT as a thermal energy source. For both charging protocols, the contribution of the PVT is approximately the same, as shown in Figs. 18(a) and 18(b). In this scenario, the energy sent from the PVT to the thermal network is one order of magnitude less than in Scenario 3. The thermal network temperature difference for both cases can explain this. As the indoor temperature in Scenario 3 is consistently lower than in Scenario 4, the temperature in the network would also be lower, allowing the PVT to provide

thermal power in lower temperatures. However, this does not prevent the indoor temperature from reaching values below the setpoint, unlike in Scenario 4, where the TESS and the HP can ensure an indoor temperature above the setpoint, requiring higher temperatures from the PVT to be able to contribute. Nevertheless, the PVT cannot reach such temperatures consistently, thus reducing the amount of thermal energy it provides to the network.

Given the small contribution of the PVT to the thermal network, this scenario becomes similar to Scenario 2 in terms of thermal power flow. Figs. 18(c) and 18(d) demonstrate that increasing the number of PVT modules does not affect the amount of thermal energy the HP
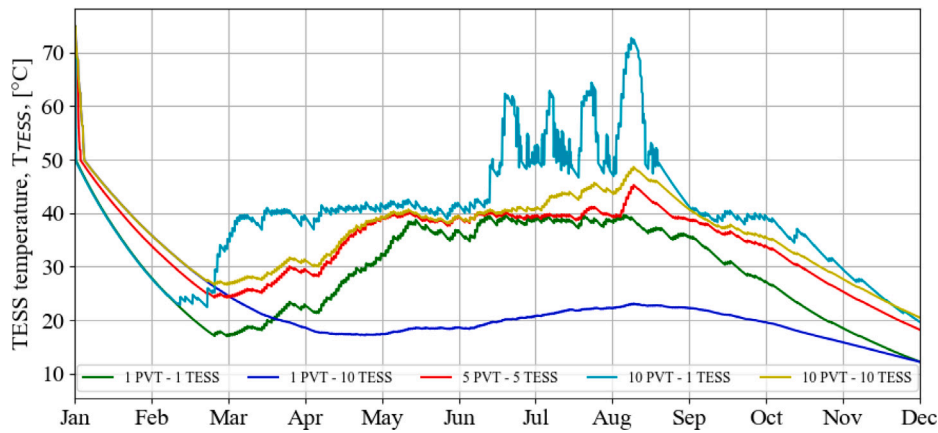
Fig. 15. Temperature in the TESS during the year for different numbers of PVT modules and TESS volumes in Scenario 3.

(a)   (b)
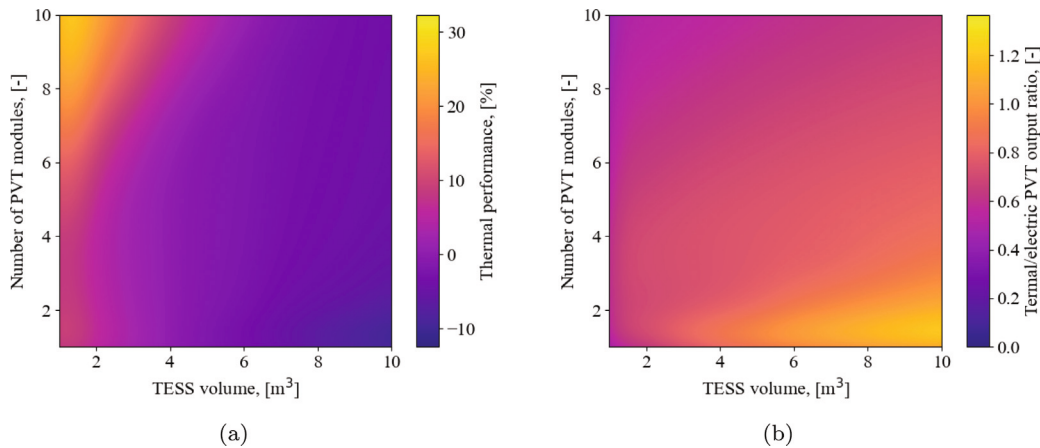
Fig. 16. Thermal performance in Scenario 3. (a) Thermal performance. (b) Ratio of the thermal and electrical output of the PVT.

provides to the TESS for any given capacity. In addition, those results and the self-discharge losses presented in Figs. 18(e) and 18(f) are approximately the same as in Scenario 2, regardless of the charging protocol. Albeit the COPs for the fully-charged protocol improve slightly, ranging between 0.88 and 0.95, the yearly average only increased to 0.89. Similarly, the COP in the cycling protocol ranged between 1.28 and 1.38. Therefore, both scenarios present comparable thermal performances to Scenario 2, as shown in Fig. 19.

The electric behavior, on the other hand, differs from the previous scenarios. In this scenario, the PVT generation is not enough to achieve a net-zero condition (see Figs. 20(a), 20(b), 20(c) and 20(d)). This also translates into less energy stored in the BESS than Scenario 3. Figs. 20(e) and 20(f) demonstrate that the increased frequency of use of the HP allows more energy to be consumed directly from the PVT instead of being stored in the BESS. Also, the convergence in the energy stored in the BESS shown in Scenario 3 no longer occurs due to the increased load. However, given the stochasticity of both the PVT generation and the HP activation, added to the limited capacity of the BESS inverter, energy is still sent back to the grid, as shown in Figs. 20(g) and 20(h).

When comparing the two protocols in this scenario, one can notice that keeping the TESS with a high SoC reduces the energy stored in the BESS and sent back to the grid. In contrast, the net energy consumption is around 30% more than with the cycling protocol. This was also present in Scenario 2, where the electric performance of the latter protocol outperformed the former. However, in Scenario 2, no energy was sent back to the grid due to the absence of PVT. This creates a dual challenge for grid operators. On the one hand, the stress in the network

increases as the energy consumption increases between four to six times with the fully-charged protocol and three to five times with the cycling protocol. On the other hand, overvoltages can occur as energy is being sent back to the grid.

3.6. Comparison

After analyzing each scenario, this section compares the advantages and disadvantages between scenarios. We considered three comparison points: thermal performance, electrical performance, and equivalent emissions. The reference point is the base case with only the gas boiler defined in Section 3.2, which always meets the thermal demand, produces 1497 kg of $CO_{2,eq}$, and has a net consumption of 2375 kWh from the grid. Table 7 presents a summary of the previous sections' results.

From the perspective of the space heating thermal demand, all scenarios except Scenario 3 ensure an indoor temperature above the setpoint temperature. The results suggest that, given the priority of the TESS over the heat pump in Scenarios 2 and 4, the contributions of the HP to the thermal demand are almost negligible. The HP is only used to keep the TESS charged when using the fully-charged protocol. In the cycling protocol, the HP provides thermal power to the network if the TESS gets discharged and thermal power is still needed. Then, the HP remains active to charge back the TESS. Nevertheless, using the HP to provide thermal power through the TESS reduces the system's thermal performance. When comparing Scenario 1 with Scenarios 2 and 4, the difference between the amount of energy generated vs. the thermal demand is noticeable. Figs. 16(a), 19(a) and 19(c) show that
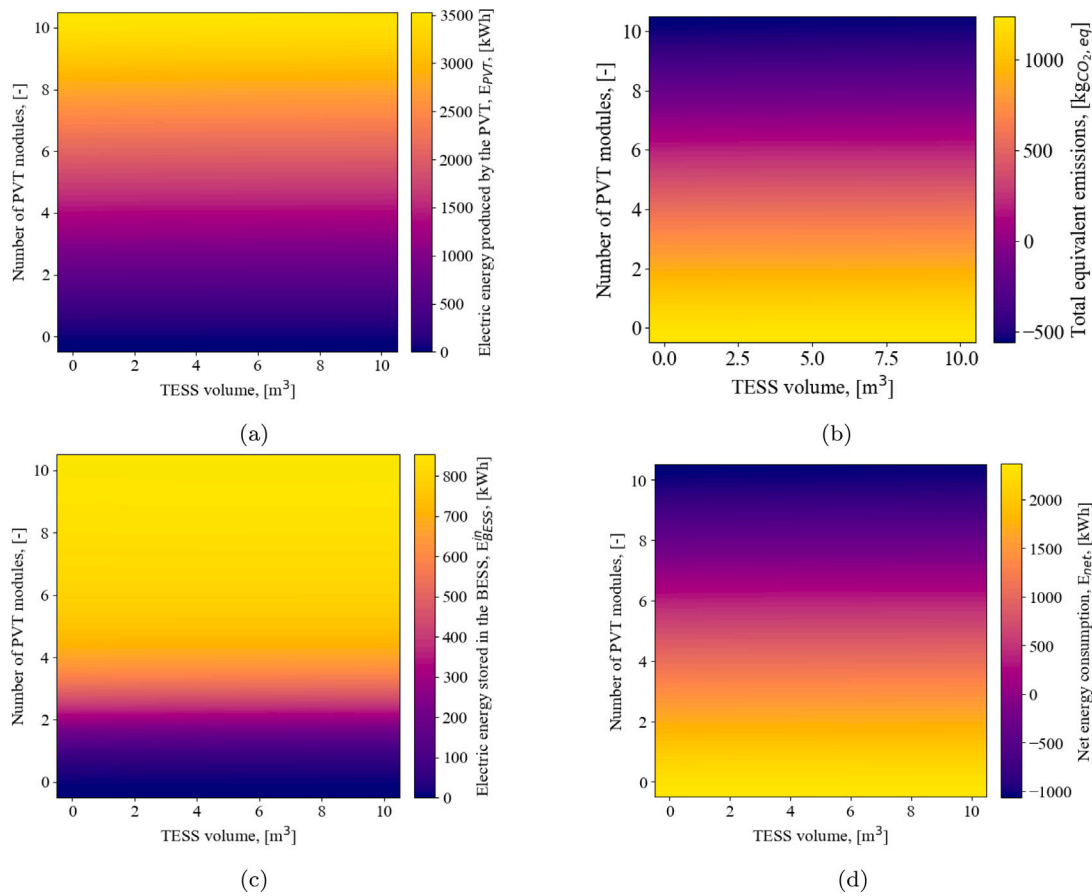
Fig. 17. Electric performance in Scenario 3. (a) PVT electric output. (b) Equivalent CO_2 emissions. (c) Energy stored in the BESS. (d) Net energy consumption from the grid.

Table 7
Summary of the results for the different scenarios.

Scenario	Architecture	TESS charge	Conclusions
Scenario I	HP	–	The $CO_{2,eq}$ produced by the HP is 1509 kg, vs 1497 kg when using the boiler, given the Dutch emission factor. The HP consumes 2886 kWh/year, with COPs ranging from 2.18 to 3.92.
Scenario II	HP and TESS	Fully-charged	The TESS loses between 684 and 4378 kWh/year to the soil and receives 11 139 to 15 159 kWh from the HP, depending on the volume (ascending), with COPs varying from 0.88 to 0.95. $CO_{2,eq}$ increases between 4654 to 7467 $kg_{CO_{2,eq}}$.
		Cycling	Loses between 533 and 3405 kWh/year to the soil and receives 11 766 to 15 905 kWh from the HP, depending on the volume (ascending), with COPs varying from 1.29 to 1.38. $CO_{2,eq}$ increases between 3087 to 4960 $kg_{CO_{2,eq}}$.
Scenario III	PVT and TESS	–	The PVT cannot charge the TESS for any combination of volumes and number of modules considered. More modules with smaller TESS capacities can keep the tank near 40 °C. However, more than seven modules would create a net-positive building, which could potentially cause instabilities in the low-voltage network.
Scenario IV	PVT, TESS and HP	Fully-charged	The PVT contribution to meet the thermal demand is below 3.25% of the total thermal energy needed; thus, the behavior of the HP is almost identical to Scenario II. The consumption of the HP prevents a net-zero building; nevertheless, up to 1587 kWh/year, depending on the number of modules, are sent back to the grid due to the storage and inverter capacities of the BESS. $CO_{2,eq}$ increases between 2784 to 7467 $kg_{CO_{2,eq}}$.
		Cycling	The PVT contribution to meet the thermal demand is below 3.25% of the total thermal energy needed; thus, the behavior of the HP is almost identical to Scenario II. The consumption of the HP prevents a net-zero building; nevertheless, up to 1708 kWh/year, depending on the number of modules, are sent back to the grid due to the storage and inverter capacities of the BESS. $CO_{2,eq}$ increases between 1217 to 4960 $kg_{CO_{2,eq}}$.
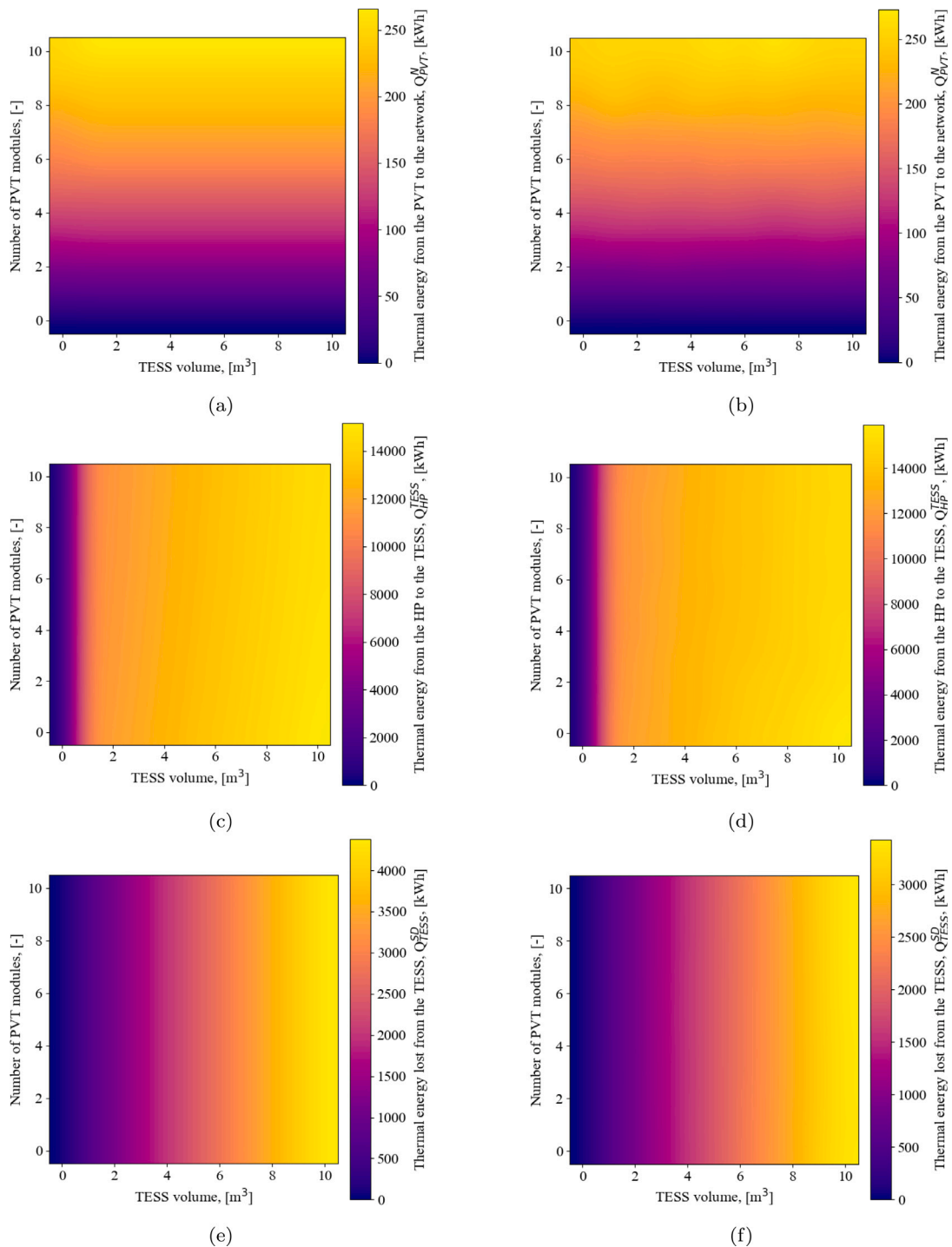
Fig. 18. Thermal power flow in Scenario 4. Thermal energy from the PVT to the thermal network using (a) the fully-charged and (b) the cycling protocol. Thermal energy from the HP to the TESS using (c) the fully-charged and (d) the cycling protocol. Energy loss to the soil due to self-discharge using (e) the fully-charged and (f) the cycling protocol.

the thermal performance is between 40 and 70% in the presence of TESS, whereas is 100% in Scenario 1.

Low thermal performance also leads to poor electric performance. In Scenario 1, the COP of the HP oscillates between 2.18 to 3.92. In contrast, Scenarios 2 and 4 have maximum COPs below 1 with the fully-charged protocol and 1.4 with the cycling protocol. This considerably augments the yearly electric energy consumption, even in Scenario 4 with the PVT, increasing the chances of undervoltages in the distribution network. Moreover, energy is returned to the grid despite using a battery energy storage system. This is undesired in most

cases, as it can lead to overvoltages and congestion in the distribution network. Therefore, Scenarios 2 and 4 represent a significant challenge for grid operators. Similarly, Scenario 3 achieves net-zero consumption, even reaching net-positive conditions. Nevertheless, the stochasticity of the PVT generation causes a bidirectional energy exchange with the grid, potentially causing congestion and more severe overvoltages than previous scenarios due to the lower energy consumption and the same energy generation.

In Section 3.2, we mentioned that, given the Dutch emission factors, an improvement in $CO_{2,eq}$ from the base case with the boiler can be
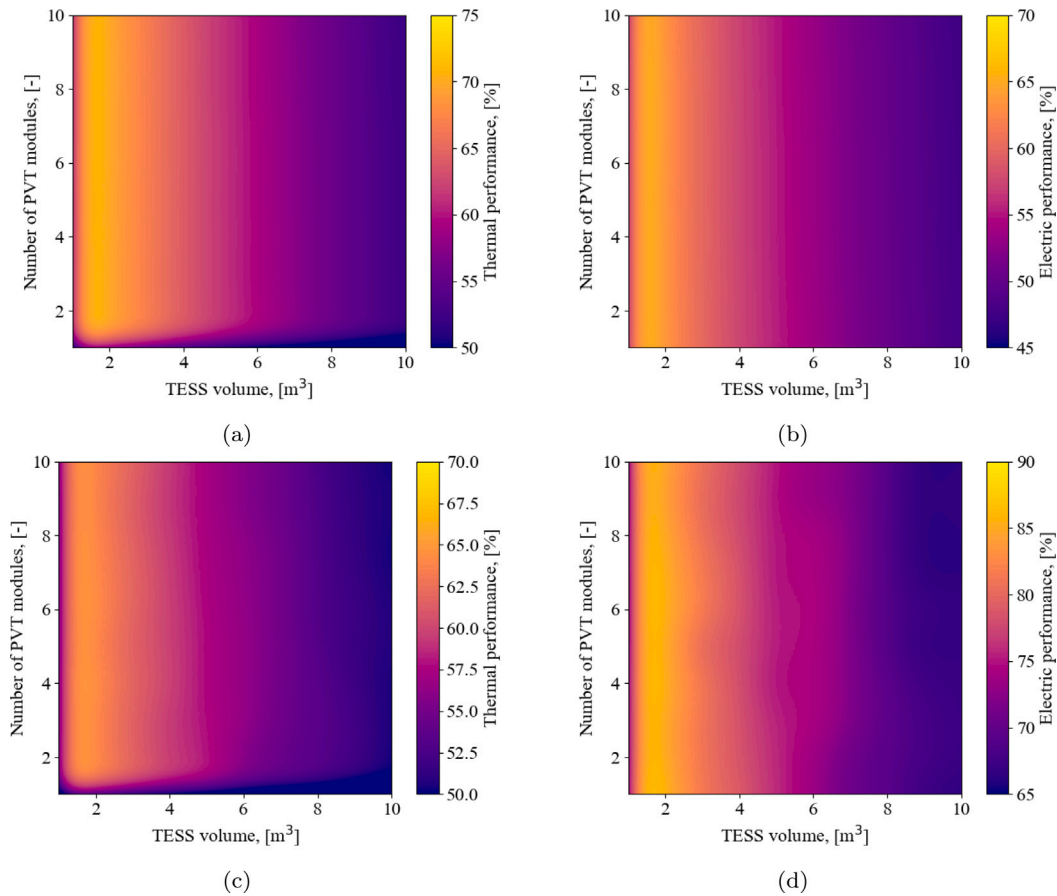
Fig. 19. Performance in Scenario 4. Thermal performance using (a) the fully-charged and (c) the cycling protocol. Electric performance using (b) the fully-charged and (d) the cycling protocol.

achieved with a net electric consumption increase below 2900 kWh/year, *i.e.*, the total net energy consumption should be 5250 kWh/year or less. Using only the heat pump, as in Scenario 1, it is possible to meet this criteria. Scenario 3 consistently reduced the net consumption from the grid at the expense of thermal comfort. In this scenario, the net energy consumption can reach even negative values, turning the house into a net-positive building when there are more than seven PVT modules, but the heat production cannot meet the thermal demand, making this scenario unfeasible. On the other hand, Scenario 4 can meet this requirement only in the case without TESS. In fact, the only difference between this case and Scenario 2 is the PVT. In Scenario 2, the absence of PVT considerably increases the equivalent emissions compared with only the HP or the gas boiler in Scenario 1, ranging from 3087 $kg_{CO_2,eq}$ more in the case with the smaller TESS, up to 4960 $kg_{CO_2,eq}$ for the cycling protocol. The equivalent emissions increase for the fully-charged protocol is worse, ranging from 4654 to 7467 $kg_{CO_2,eq}$. Scenario 4 has a lower equivalent emissions impact than Scenario 2, as the PVT can compensate for up to 1870 $kg_{CO_2,eq}$ when using 10 modules, but it is insufficient to justify the usage of the TESS from an emissions perspective. It was also demonstrated that the PVT does not provide any significant advantage on the thermal side. For this reason, a PV system would add the same value towards reducing the equivalent emissions, with a lower cost, as it would not require the hydraulic components. Then, adding thermal storage increased several times the electrical consumption, thus, the $CO_{2,eq}$.

Assuming the same weight for the three criteria, Scenario 1 shows the best performance overall. This scenario can meet the thermal demand with the lower electric and net grid consumption; therefore, its $CO_{2,eq}$ is just below Scenario 3. Scenarios 2 and 4 have almost the same thermal performance; however, Scenario 4 has better electric

behavior from the user perspective due to the solar energy from the PVT, reducing its $CO_{2,eq}$. Still, from the grid perspective, Scenario 4 represents the most significant challenge among the four scenarios due to the notable increase in consumption and stochastic bidirectional energy flow. Scenario 3 outperforms the other scenarios in the net grid consumption, but it cannot meet the thermal demand, which makes it an unsuitable architecture. Notably, all scenarios can provide ancillary services if the multi-carrier system is sized according to a specific ancillary service, such as voltage control or congestion management, and an adequate EMS strategy is implemented. If so, Scenarios 2 or 4 might become more attractive than Scenario 1, thanks to the combination of the HP and the TESS. For instance, variable energy prices would make it more profitable to use the heat pump when heating demand is not necessarily needed, thus requiring thermal energy storage, resulting in a cost-driven demand response. Similarly, using the heat pump to charge the TESS in high-power injection periods despite no heating being needed could potentially support the grid in reducing overvoltages without affecting the thermal comfort of the occupants of the house.

4. Conclusions

In this work, we described analytical models for the elements of a multi-carrier energy system to replace gas boilers for space heating in residential houses in the Netherlands. We used an underground water tank thermal energy storage system for our analysis, providing a analytical model to estimate its self-discharge to the surrounding soil. Then, we evaluated four architecture scenarios to determine their electrical consumption from the grid, thermal power generation for space heating and $CO_{2,eq}$ emissions. We demonstrated that using a heat
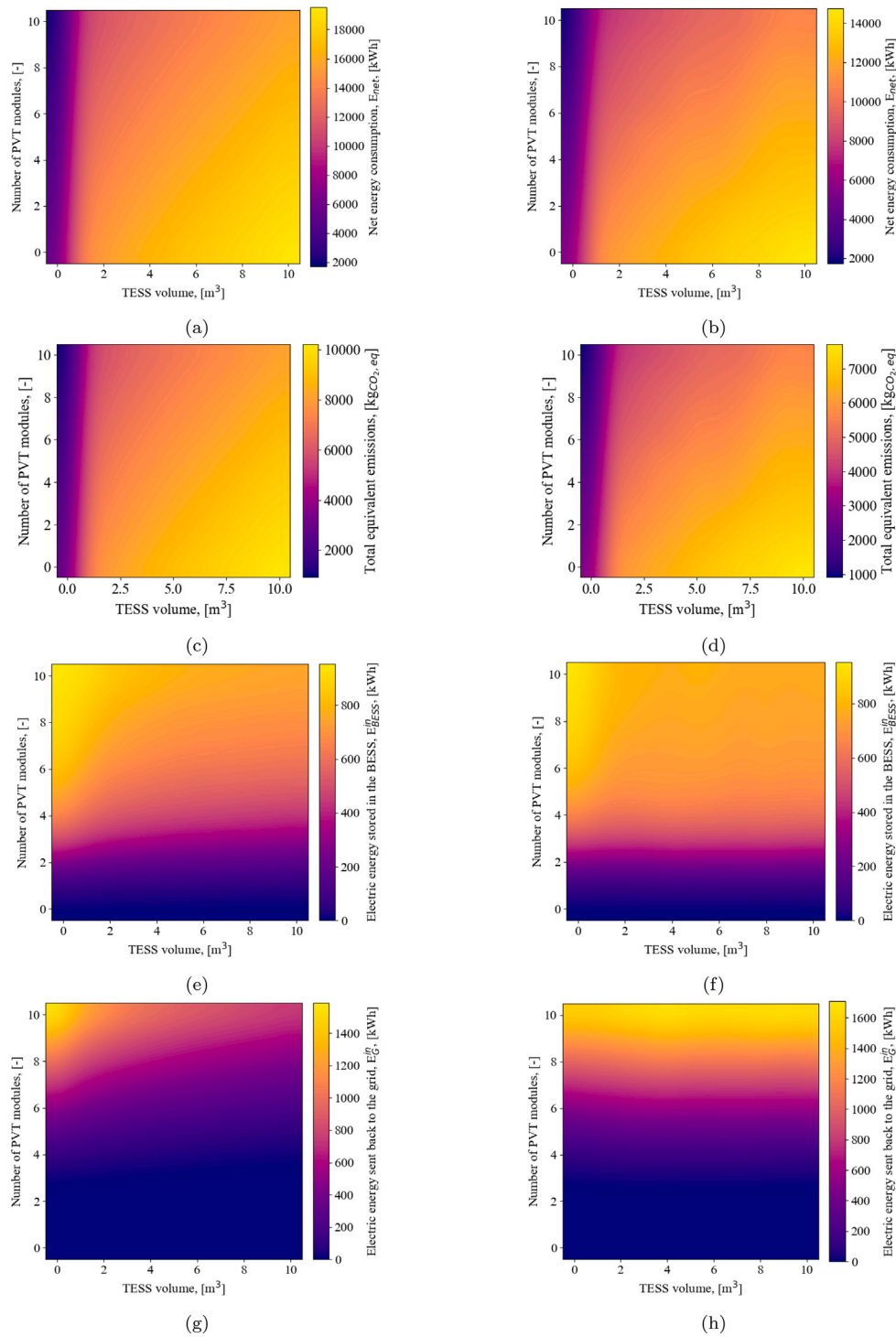
Fig. 20. Electric energy flow in Scenario 4. Net energy consumption from the grid when using (a) the fully-charged and (b) the cycling protocol. Equivalent CO_2 emissions when using (c) the fully-charged and (d) the cycling protocol. Energy stored in the BESS when using (e) the fully-charged and (f) the cycling protocol. Energy returned to the grid when using (g) the fully-charged and (h) the cycling protocol.

pump generates approximately the same equivalent emissions as the gas boiler in households (around 1500 kg of $CO_{2,eq}$); however, a more renewable network would improve the heat pump result. Coupling a PVT to the heat pump did not provide any value from the thermal perspective; thus, a PV system could be used instead if the target is a net-zero building at the cost of more stochasticity added to the grid.

We also proved the incompatibility of water tank TESS and PVT systems due to the low temperature the latter can generate. When coupled with a heat pump, the electrical consumption, thus, the $CO_{2,eq}$,

increased from three to six times than when using the heat pump alone. This is because the temperature difference between the fluid stored in the TESS (50–95 °C) and the ambient (−5–30 °C) reduces the COP to values near 1, regardless of the charging cycle. It was noted, however, that using the cycling protocol reduces the frequency of activation of the heat pump to charge the tank. This way, the TESS is capable of providing enough thermal power for space heating independently, but the overall performance of the HP coupled the TESS depends on the charging and discharging strategy. Such strategies could provide

flexibility in a scenario where the TESS does not depend solely on the HP to charge, as adding the HP consistently increases the energy consumption and adds power peaks to the base demand. Combining with PVT systems can reduce the net energy consumption from the grid, but it could contribute to voltage stability issues for grid operators given the amount of electrical power injected into the grid.

CRediT authorship contribution statement

Joel Alpízar-Castillo: Conceptualization, Formal analysis, Investigation, Methodology, Software, Writing – original draft. **Laura M. Ramírez-Elizondo:** Funding acquisition, Supervision, Writing – review & editing. **Pavol Bauer:** Funding acquisition, Project administration, Writing – review & editing.

Declaration of competing interest

The authors declare the following financial interests/personal relationships which may be considered as potential competing interests: Pavol Bauer reports financial support was provided by Netherlands Enterprise Agency. If there are other authors, they declare that they have no known competing financial interests or personal relationships that could have appeared to influence the work reported in this paper.

Data availability

Data will be made available on request.

Acknowledgment

References

[1] The Netherlands 2020 - energy policy review. Technical Report, International Energy Agency; 2020, URL https://iea.blob.core.windows.net/assets/93f03b36-64a9-4366-9d5f-0261d73d68b3/The_Netherlands_2020_Energy_Policy_Review.pdf.

[2] Oei A, Haffner R, van Til H, Heidecke L, Slaakweg A. Van CV-ketel naar duurzame warmte - Twee toekomstbeelden voor een warme Nederlandse gebouwde omgeving in 2030. Technical Report, Ecorys; 2018, URL https://iea.blob.core.windows.net/assets/93f03b36-64a9-4366-9d5f-0261d73d68b3/The_Netherlands_2020_Energy_Policy_Review.pdf.

[3] Geraedts M, Alpízar-Castillo J, Ramírez-Elizondo L, Bauer P. Optimal sizing of a community level thermal energy storage system. In: 2022 IEEE 21st mediterranean electrotechnical conference. MELECON, 2022, p. 52–7. http://dx.doi.org/10.1109/MELECON53508.2022.9842945.

[4] Oh J, Bae S, Chae H, Jeong J, Nam Y. Photovoltaic–thermal advanced technology for real applications: Review and case study. Energy Rep 2023;10:1409–33. http://dx.doi.org/10.1016/j.egyr.2023.08.002, URL https://www.sciencedirect.com/science/article/pii/S2352484723011435.

[5] Tiwari AK, Chatterjee K, Agrawal S, Singh GK. A comprehensive review of photovoltaic thermal (PVT) technology: Performance evaluation and contemporary development. Energy Rep 2023;10:2655–79. http://dx.doi.org/10.1016/j.egyr.2023.09.043, URL https://www.sciencedirect.com/science/article/pii/S2352484723012878.

[6] Ranjbar Golafshani S, Fatehpour M, Houshfar E. Optimization and dynamic techno-economic assessment of integrated combined ejector cooling, heating, and power system. Energy 2023;282:128829. http://dx.doi.org/10.1016/j.energy.2023.128829, URL https://www.sciencedirect.com/science/article/pii/S0360544223022235.

[7] Kallio S, Siroux M. Hybrid renewable energy systems based on micro-cogeneration. Energy Rep 2022;8:762–9. http://dx.doi.org/10.1016/j.egyr.2021.11.158, URL https://www.sciencedirect.com/science/article/pii/S2352484721013056, 2021 The 8th International Conference on Power and Energy Systems Engineering.

[8] Herre L, Nourozi B, Hesamzadeh MR, Wang Q, Söder L. Provision of multiple services with controllable loads as multi-area thermal energy storage. J Energy Storage 2023;63:107062. http://dx.doi.org/10.1016/j.est.2023.107062, URL https://www.sciencedirect.com/science/article/pii/S2352152X23004590.

[9] Wang S, Hoes P-J, Hensen JLM, Adan OCG, Donkers PAJ. Investigating the use cases of a novel heat battery in Dutch residential buildings. Build Simul 2023;16(9):1675–89. http://dx.doi.org/10.1007/s12273-023-1069-2, URL https://www.scopus.com/inward/record.uri?eid=2-s2.0-85168571099&doi=10.1007%2fs12273-023-1069-2&partnerID=40&md5=ef6d91aebc5a9fbf21a8f6bb9bc74653.

[10] Clift DH, Leerson J, Hasan KN, Rosengarten G. Maximising the benefit of variable speed heat-pump water heater with rooftop PV and intelligent battery charging. Sol Energy 2023;265. http://dx.doi.org/10.1016/j.solener.2023.112049, URL https://www.scopus.com/inward/record.uri?eid=2-s2.0-85175805870&doi=10.1016%2fj.solener.2023.112049&partnerID=40&md5=79f575686dac560ddc40886c0670d95e.

[11] Hirschey J, Li Z, Gluesenkamp KR, LaClair TJ, Graham S. Demand reduction and energy saving potential of thermal energy storage integrated heat pumps. Int J Refrig 2023;148:179–92. http://dx.doi.org/10.1016/j.ijrefrig.2023.01.026, URL https://www.sciencedirect.com/science/article/pii/S0140700723000348.

[12] Torricelli N, Branchini L, De Pascale A, Dumont O, Lemort V. Optimal management of reversible heat pump/organic rankine cycle carnot batteries. J Eng Gas Turbines Power 2023;145(4). http://dx.doi.org/10.1115/1.4055708, URL https://www.scopus.com/inward/record.uri?eid=2-s2.0-85159203479&doi=10.1115%2f1.4055708&partnerID=40&md5=6f62e158e318bf645891797ddd6a4bac.

[13] Ramos A, Chatzopoulou MA, Guarracino I, Freeman J, Markides CN. Hybrid photovoltaic thermal solar systems for combined heating, cooling and power provision in the urban environment. Energy Convers Manage 2017;150:838–50. http://dx.doi.org/10.1016/j.enconman.2017.03.024, URL https://www.sciencedirect.com/science/article/pii/S0196890417302273.

[14] Emamjome Kashan M, Fung AS, Swift J. Integrating novel microchannel-based solar collectors with a water-to-water heat pump for cold-climate domestic hot water supply, including related solar systems comparisons. Energies 2021;14(13). http://dx.doi.org/10.3390/en14134057, URL https://www.mdpi.com/1996-1073/14/13/4057.

[15] Navakrishnan S, Vengadesan E, Senthil R, Dhanalakshmi S. An experimental study on simultaneous electricity and heat production from solar PV with thermal energy storage. Energy Convers Manage 2021;245:114614. http://dx.doi.org/10.1016/j.enconman.2021.114614, URL https://www.sciencedirect.com/science/article/pii/S0196890421007901.

[16] Carmona M, Palacio Bastos A, García JD. Experimental evaluation of a hybrid photovoltaic and thermal solar energy collector with integrated phase change material (PVT-PCM) in comparison with a traditional photovoltaic (PV) module. Renew Energy 2021;172:680–96. http://dx.doi.org/10.1016/j.renene.2021.03.022, URL https://www.sciencedirect.com/science/article/pii/S0960148121003761.

[17] Selimefendigil F, Şirin C. Energy and exergy analysis of a hybrid photovoltaic/thermal-air collector modified with nano-enhanced latent heat thermal energy storage unit. J Energy Storage 2022;45:103467. http://dx.doi.org/10.1016/j.est.2021.103467, URL https://www.sciencedirect.com/science/article/pii/S2352152X21011518.

[18] Fischer D, Byskov-Linbder K, Flunk A, Wille-Haussmann B, Kreifels N, Scherer J. Impact of HP, CHP, PV and EVs on households' electric load profiles. 2015, http://dx.doi.org/10.1109/PTC.2015.7232784.

[19] Mitterrutzner B, Callegher CZ, Fraboni R, Wilczynski E, Pezzutto S. Review of heating and cooling technologies for buildings: A techno-economic case study of eleven European countries. Energy 2023;284:129252. http://dx.doi.org/10.1016/j.energy.2023.129252, URL https://www.sciencedirect.com/science/article/pii/S0360544223026464.

[20] Cui P, Yang W, Zhang W, Zhu K, Spitler JD, Yu M. Advances in ground heat exchangers for space heating and cooling: Review and perspectives. Energy Built Environ 2024;5(2):255–69. http://dx.doi.org/10.1016/j.enbenv.2022.10.002, URL https://www.sciencedirect.com/science/article/pii/S2666123322000733.

[21] Konrad ME, MacDonald BD. Cold climate air source heat pumps: Industry progress and thermodynamic analysis of market-available residential units. Renew Sustain Energy Rev 2023;188:113739. http://dx.doi.org/10.1016/j.rser.2023.113739, URL https://www.sciencedirect.com/science/article/pii/S1364032123005968.

[22] Ji L, Shukla SK, Zuo Z, Lu X, Ji X, Wang C. An overview of the progress of new working pairs in absorption heat pumps. Energy Rep 2023;9:703–29. http://dx.doi.org/10.1016/j.egyr.2022.11.143, URL https://www.sciencedirect.com/science/article/pii/S235248472202532X.

[23] Alpízar-Castillo J, Ramírez-Elizondo L, Bauer P. The effect of non-coordinated heating electrification alternatives on a low-voltage distribution network with high PV penetration. In: 2023 IEEE 17th international conference on compatibility, power electronics and power engineering (CPE-POWEREnG). 2023, p. 1–6. http://dx.doi.org/10.1109/CPE-POWERENG58103.2023.10227394.

[24] Foslie SS, Knudsen BR, Korpås M. Integrated design and operational optimization of energy systems in dairies. Energy 2023;281:128242. http://dx.doi.org/10.1016/j.energy.2023.128242, URL https://www.sciencedirect.com/science/article/pii/S0360544223016365.

[25] Alpízar-Castillo J, Ramirez-Elizondo L, Bauer P. Assessing the role of energy storage in multiple energy carriers toward providing ancillary services: A review. Energies 2023;16(1). http://dx.doi.org/10.3390/en16010379, URL https://www.mdpi.com/1996-1073/16/1/379.

[26] Kumar S, Kaur T, Arora M, Upadhyay S. Resource estimation and sizing optimization of PV/micro hydro-based hybrid energy system in rural area of Western Himalayan Himachal Pradesh in India. Energy Sources A: Recov Utiliz Environ Effects 2019;41(22):2795–807. http://dx.doi.org/10.1080/15567036.2019.1576075, URL https://www.scopus.com/inward/record.uri?eid=2-s2.0-85061595587&doi=10.1080%2f15567036.2019.1576075&partnerID=40&md5=be32f8d9edb240a160a2d270774a4d5a.

[27] Barbu M, Minciuc E, Frusescu DC, Tutica D. Integration of hybrid photovoltaic thermal panels (PVT) in the district heating system of bucharest, Romania. In: 2021 10th international conference on ENERGY and ENVIROnMENT. CIEM, 2021, p. 1–5. http://dx.doi.org/10.1109/CIEM52821.2021.9614721.

[28] Jafari M, Armaghan D, Seyed Mahmoudi S, Chitsaz A. Thermoeconomic analysis of a standalone solar hydrogen system with hybrid energy storage. Int J Hydrogen Energy 2019;44(36):19614–27. http://dx.doi.org/10.1016/j.ijhydene.2019.05.195, URL https://www.sciencedirect.com/science/article/pii/S036031991932110X.

[29] Zhou C, Liang R, Zhang J, Riaz A. Experimental study on the cogeneration performance of roll-bond-PVT heat pump system with single stage compression during summer. Appl Therm Eng 2019;149:249–61. http://dx.doi.org/10.1016/j.applthermaleng.2018.11.120, URL https://www.scopus.com/inward/record.uri?eid=2-s2.0-85058216317&doi=10.1016%2fj.applthermaleng.2018.11.120&partnerID=40&md5=cb00d57a24d8cce4e5e2d028f65229fa.

[30] Hengel F, Heschl C, Inschlag F, Klanatsky P. System efficiency of pvt collector-driven heat pumps. Int J Thermofluids 2020;5–6. http://dx.doi.org/10.1016/j.ijft.2020.100034, URL https://www.scopus.com/inward/record.uri?eid=2-s2.0-85090992055&doi=10.1016%2fj.ijft.2020.100034&partnerID=40&md5=c4cc85a8fa056218c11fea222f8fc3c0.

[31] Jiang L, Liu W, Lin Y, Wang R, Zhang X, Hu M. Hybrid thermochemical sorption seasonal storage for ultra-low temperature solar energy utilization. Energy 2022;239. http://dx.doi.org/10.1016/j.energy.2021.122068, URL https://www.scopus.com/inward/record.uri?eid=2-s2.0-85115611628&doi=10.1016%2fj.energy.2021.122068&partnerID=40&md5=484c3650ea585574f9fa7ac178bb20c3.

[32] Renaldi R, Kiprakis A, Friedrich D. An optimisation framework for thermal energy storage integration in a residential heat pump heating system. Appl Energy 2017;186:520–9. http://dx.doi.org/10.1016/j.apenergy.2016.02.067, URL https://www.scopus.com/inward/record.uri?eid=2-s2.0-84959144692&doi=10.1016%2fj.apenergy.2016.02.067&partnerID=40&md5=164f2c5cc2b54592e159df2d5315749d.

[33] Aunedi M, Strbac G. System benefits of residential heat storage for electrified heating sector in the United Kingdom. In: 2022 IEEE PES innovative smart grid technologies conference europe (ISGT-europe). 2022, p. 1–5. http://dx.doi.org/10.1109/ISGT-Europe54678.2022.9960709.

[34] Vallati A, Fiorini CV, Basso GL, Muzi F, Oclon P, di Matteo M. Optimization of a thermal storage tank for a water water heat pump solar assited. In: 2023 8th international conference on smart and sustainable technologies (spliTech). 2023, p. 1–7. http://dx.doi.org/10.23919/SpliTech58164.2023.10192989.

[35] ur Rehman H, Hasan A, Reda F. Challenges in reaching positive energy building level in apartment buildings in the Nordic climate: A techno-economic analysis. Energy Build 2022;262:111991. http://dx.doi.org/10.1016/j.enbuild.2022.111991, URL https://www.sciencedirect.com/science/article/pii/S0378778822001621.

[36] Kim M-H, An Y, Joo H-J, Lee D-W, Yun J-H. Self-sufficiency and energy savings of renewable thermal energy systems for an energy-sharing community. Energies 2021;14(14). http://dx.doi.org/10.3390/en14144284, URL https://www.scopus.com/inward/record.uri?eid=2-s2.0-85111145535&doi=10.3390%2fen14144284&partnerID=40&md5=8d86a6a39d721dc97d12c99741139f05.

[37] Herrando M, Ramos A, Freeman J, Zabalza I, Markides CN. Technoeconomic modelling and optimisation of solar combined heat and power systems based on flat-box PVT collectors for domestic applications. Energy Convers Manage 2018;175:67–85. http://dx.doi.org/10.1016/j.enconman.2018.07.045, URL https://www.scopus.com/inward/record.uri?eid=2-s2.0-85052890685&doi=10.1016%2fj.enconman.2018.07.045&partnerID=40&md5=bef699b640829fcb05004208045171d1.

[38] Abdul-Ganiyu S, Quansah DA, Ramde EW, Seidu R, Adaramola MS. Techno-economic analysis of solar photovoltaic (PV) and solar photovoltaic thermal (PVT) systems using exergy analysis. Sustain Energy Technol Assess 2021;47. http://dx.doi.org/10.1016/j.seta.2021.101520, URL https://www.scopus.com/inward/record.uri?eid=2-s2.0-85112290300&doi=10.1016%2fj.seta.2021.101520&partnerID=40&md5=b8fea69671b51d40b62e83e061b272f7.

[39] Gholami H, Khalilnejad A, Gharehpetian G. Electrothermal performance and environmental effects of optimal photovoltaic thermal system. Energy Convers Manage 2015;95:326–33. http://dx.doi.org/10.1016/j.enconman.2015.02.014, URL https://www.scopus.com/inward/record.uri?eid=2-s2.0-84923829852&doi=10.1016%2fj.enconman.2015.02.014&partnerID=40&md5=321094fe41a1066dc1e00be6483c66ef.

[40] Rostmnezhad Z, Dessaint L. Power management in smart buildings using reinforcement learning. In: 2023 IEEE power and energy society innovative smart grid technologies conference, ISGT 2023. 2023, http://dx.doi.org/10.1109/ISGT51731.2023.10066398, URL https://www.scopus.com/inward/record.uri?eid=2-s2.0-85151492082&doi=10.1109%2fISGT51731.2023.10066398&partnerID=40&md5=912d89ca3b23d400b11eea364f2285e0.

[41] Brahman F, Honarmand M, Jadid S. Optimal electrical and thermal energy management of a residential energy hub, integrating demand response and energy storage system. Energy Build 2015;90:65–75. http://dx.doi.org/10.1016/j.enbuild.2014.12.039, URL https://www.scopus.com/inward/record.uri?eid=2-s2.0-84921518001&doi=10.1016%2fj.enbuild.2014.12.039&partnerID=40&md5=6f5d8664031effe100a8444f8710494d.

[42] Koch M, Dott R. Contributions to system integration of PV and PVT collectors with heat pumps in buildings. E3S Web Conf 2019;111:01061. http://dx.doi.org/10.1051/e3sconf/201911101061.

[43] Izquierdo M, de Agustín-Camacho P. Solar heating by radiant floor: Experimental results and emission reduction obtained with a micro photovoltaic–heat pump system. Appl Energy 2015;147:297–307. http://dx.doi.org/10.1016/j.apenergy.2015.03.007, URL https://www.sciencedirect.com/science/article/pii/S0306261915002913.

[44] Hyvönen J, Santasalo-Aarnio A, Syri S, Lehtonen M. Feasibility study of energy storage options for photovoltaic electricity generation in detached houses in Nordic climates. J Energy Storage 2022;54. http://dx.doi.org/10.1016/j.est.2022.105330, URL https://www.scopus.com/inward/record.uri?eid=2-s2.0-85134710899&doi=10.1016%2fj.est.2022.105330&partnerID=40&md5=d5665bbeee430c39dc8051c285996c23.

[45] Efkarpidis NA, Christoforidis GC, Papagiannis GK. Assessment of energy management strategies in buildings equipped with modulating heat pumps. In: SyNERGY MED 2022 - 2nd international conference on energy transition in the Mediterranean Area, proceedings. 2022, http://dx.doi.org/10.1109/SyNERGYMED55767.2022.9941406, URL https://www.scopus.com/inward/record.uri?eid=2-s2.0-85142886916&doi=10.1109%2fSyNERGYMED55767.2022.9941406&partnerID=40&md5=7c16a1608c0d12b14362a7cd758d1b42.

[46] Banaei M, D'Ettorre F, Ebrahimy R, Blomgren EMV, Madsen H. Mutual impacts of procuring energy flexibility and equipment degradation at the residential consumers level. In: 2021 IEEE PES innovative smart grid technologies europe (ISGT europe). 2021, p. 1–6. http://dx.doi.org/10.1109/ISGTEurope52324.2021.9640142.

[47] Fuentes E, Arce L, Salom J. A review of domestic hot water consumption profiles for application in systems and buildings energy performance analysis. Renew Sustain Energy Rev 2018;81:1530–47. http://dx.doi.org/10.1016/j.rser.2017.05.229, URL https://www.sciencedirect.com/science/article/pii/S1364032117308614.

[48] EN standard 806-3 - specification for installations inside buildings conveying water for human consumption. 2012.

[49] Pothof I, Vreeken T, van Meerkerk M. Field measurements on lower radiator temperatures in existing buildings. 2022, URL https://www.warmingup.info/documenten/11205149-hye-001_field-measurements-on-lower-radiator-temperatures-in-existing-buildings_def.pdf.

[50] American Society of Heating, Refrigerating and Air-Conditioning Engineers, Inc(ASHRAE). 2021 ASHRAE® Handbook - Fundamentals (SI Edition). American Society of Heating, Refrigerating and Air-Conditioning Engineers, Inc. (ASHRAE); 2021.

[51] Singh RK, Sharma RV. Numerical analysis for ground temperature variation. Geotherm Energy 2017;5(1). URL https://geothermal-energy-journal.springeropen.com/articles/10.1186/s40517-017-0082-z.

[52] Hillel D, editor. Composite phenomena. In: Introduction to environmental soil physics. Burlington: Academic Press; 2003, p. xi. http://dx.doi.org/10.1016/B978-012348655-4/50000-9, URL https://www.sciencedirect.com/science/article/pii/B9780123486554500009.

[53] Wong RY, Tso C, Jeong S, Fu S, Chao CY. Critical sky temperatures for passive radiative cooling. Renew Energy 2023;211:214–26. http://dx.doi.org/10.1016/j.renene.2023.04.142, URL https://www.sciencedirect.com/science/article/pii/S0960148123006080.

[54] Barbu M, Siroux M, Darie G. Numerical model and parametric analysis of a liquid based hybrid photovoltaic thermal (PVT) collector. Energy Rep 2021;7:7977–88. http://dx.doi.org/10.1016/j.egyr.2021.07.058, URL https://www.sciencedirect.com/science/article/pii/S2352484721005242.

[55] Wai Zhe L, Yusoff M, Ibrahim S, Irwanto M, Amelia A, Zhubir N, et al. Simulation study on photovoltaic panel temperature under different solar radiation using computational fluid dynamic method. J Phys Conf Ser 2020;1432:012052. http://dx.doi.org/10.1088/1742-6596/1432/1/012052.

[56] Damianakis N, Mouli GCR, Bauer P. Risk-averse estimation of electric heat pump power consumption. In: 2023 IEEE 17th international conference on compatibility, power electronics and power engineering (CPE-POWEREnG). 2023, p. 1–6. http://dx.doi.org/10.1109/CPE-POWERENG58103.2023.10227424.

[57] Pipattanasomporn M, Kuzlu M, Rahman S, Teklu Y. Load profiles of selected major household appliances and their demand response opportunities. IEEE Trans Smart Grid 2014;5(2):742–50. http://dx.doi.org/10.1109/TSG.2013.2268664.

[58] Alpízar-Castillo J, Vega-Garita V, Narayan N, Ramirez-Elizondo L. Open-access model of a PV-BESS system: Quantifying power and energy exchange for peak-shaving and self consumption applications. Energies 2023;16(14). http://dx.doi.org/10.3390/en16145480, URL https://www.mdpi.com/1996-1073/16/14/5480.

[59] KNMI. Uurgegevens van het weer in Nederland. 2022, URL https://www.knmi.nl/nederland-nu/klimatologie/uurgegevens.

[60] Energie SD. Duurzame warmte, de technieken van de warmtetransitie. 2019, URL https://servicepuntduurzameenergie.nl/wp-content/uploads/2019/10/Duurzame-warmte.pdf.

[61] van der Veen C. Analysing thermal energy storage in residential buildings: Towards decarbonization of the heating sector. (Master's thesis), The Netherlands: Technische Universiteit Delft; 2022, URL https://repository.tudelft.nl/islandora/object/uuid:c1fca7b7-a7cb-4ddc-936e-239a8f0a6cb7?collection=education.

[62] van Esch JM. BTM+ model and Expert tool. 2022, URL https://backend.tkiwatertechnologie.nl/wp-content/uploads/2020/10/Engine-BTM-and-EXPERT.pdf.

[63] Veldkamp JG, Hegen D. Temperature modelling of the dutch subsurface at the depth of the Dinantian. 2020, URL https://www.nlog.nl/sites/default/files/2020-04/SCAN%20Dinantian%20Temperature%20modelling%20Dutch%20subsurface%20at%20depth%20Dinantian%20report.pdf.